geotechnics

MDPI

Article

Numerical Investigation of Inclined Piles under Liquefaction-Induced Lateral Spreading

Yu Wang and Rolando P. Orense *

Department of Civil & Environmental Engineering, University of Auckland, Auckland 1010, New Zealand; ywan833@aucklanduni.ac.nz
* Correspondence: r.orense@auckland.ac.nz

Abstract: Inclined piles have been widely applied as one of the countermeasures against large lateral spreading induced by soil liquefaction during earthquakes. However, the unsatisfactory performance of inclined piles in past events has impeded their application in seismic areas. To elucidate the performance of inclined piles when subjected to lateral spreading induced by soil liquefaction, numerical analyzes were performed using the OpenSees framework. For this purpose, a comprehensive three-dimensional finite element model was developed. Interface elements were used between the soil and the pile to account for the friction and gapping mechanisms. A multi-yield-surface plasticity constitutive relationship for sand was adopted to simulate the soil liquefaction behavior. Based on the proposed numerical model, parametric analyzes were conducted to investigate the influence of various factors on the behavior of inclined piles, including the raked angle of the pile, the ground slope, the soil profile, and the amplitude of the input motion. The response of the system indicates that inclined piles can behave better than vertical piles in decreasing soil deformation and the cap response. The influences of the investigated factors are highlighted to adopt the appropriate pile inclination in laterally spreading ground and maximize the advantages of using inclined piles.

Keywords: inclined pile; liquefaction; lateral spreading; soil–pile interaction; OpenSees

Citation: Wang, Y.; Orense, R.P. Numerical Investigation of Inclined Piles under Liquefaction-Induced Lateral Spreading. *Geotechnics* **2023**, *3*, 320–346. https://doi.org/10.3390/geotechnics3020019

Academic Editor: Raffaele Di Laora

Received: 27 March 2023
Revised: 28 April 2023
Accepted: 2 May 2023
Published: 6 May 2023

1. Introduction

Lateral spreading has been recognized as one of the prominent contributors to damage in the pile foundations supporting bridges and offshore constructions during large-scale earthquakes, such as the 1989 Loma Prieta earthquake [1], and the 1995 Kobe earthquake [2]. Although inclined piles are widely applied to resist significant horizontal loadings, their suboptimal performance during previous earthquakes has discouraged their utilization in seismic design codes or standards (e.g., [3,4]). For instance, inclined piles exhibited poor behavior in the damaged bridges during the 2010–2011 Christchurch earthquake sequence [5] and damaged the wharf structures in the 1989 Loma Prieta earthquake [1]. Pender [6] concluded that the disappointing seismic performance of the inclined piles could be attributed to the graphical design methods utilized in earlier eras to estimate pile loads. Gerolymos et al. [7] identified several frequently mentioned disadvantages of inclined piles, including residual bending moment due to pre- and post-earthquake soil consolidation and settlement, reduction in the flexural capacity from the developed tensile axial forces, significant kinematic force, and undesirable rotation at the pile-cap connection.

Based on recent field studies and laboratory tests, the advantages of inclined piles have been recognized. In particular, the effectiveness of inclined piles against lateral spreading has been observed in a field study of the Landing Road Bridge after the 1987 Edgecumbe earthquake [8]. Additionally, inclined piles have been shown to positively impact the dynamic behavior of the soil–pile system in various seismic experiments conducted in dry sand (e.g., [9–12]). In the experiments performed by McManus et al. [13] and Shahrour and Juran [14], the use of inclined micro-piles in saturated soils has also been proven to be

beneficial in restraining soil deformation and preventing a significant excess in pore water pressure build-up. Nevertheless, further laboratory studies are still required to investigate the seismic performance of the inclined piles in liquefiable soils.

Numerous experimental and numerical studies have investigated the performance of vertical piles against lateral spreading. In terms of numerical investigations, in addition to the commonly used Beam-on-Nonlinear-Winkler-Foundation approach (e.g., [15–17]), the three-dimensional (3D) finite element method has also been extensively employed. McGann et al. [18] proposed *p-y* relationships in modeling the pile behavior against liquefaction-induced lateral spreading through 3D modeling. Cubrinovski et al. [19] and Li and Motamed [20], simulated the behavior of vertical pile groups behind waterfront structures using 3D and 2D methods, respectively. Chang et al. [21] and Cheng and Jeremić [22], investigated the behaviors of the soil–pile–superstructure systems in sloping grounds numerically. However, when dealing with inclined piles, many numerical studies focused on their performance when subjected to monotonic or dynamic loads on the pile head (e.g., [23–25]). There are also some simulations of the response of the inclined piles under dynamic loading. For instance, Gerolymos et al. [7], Giannakou et al. [26], Sadek and Shahrour [27], and Sarkar et al. [28] investigated the seismic response of the pile groups consisting of inclined piles installed in elastic soil deposits. Rajeswari and Sarkar [29] and Wang and Orense [30], conducted parametric analysis to study the seismic behavior of the inclined pile groups with consideration of soil liquefaction. In these studies, the beneficial effects of inclined piles on the response of the soil–pile system were observed. However, the performance of inclined piles against liquefaction-induced lateral spreading has not yet been fully confirmed.

To elucidate the seismic performance of the inclined piles when subjected to liquefaction-induced lateral spreading, a parametric analysis of a 3D finite element model (FEM) was carried out through the OpenSees platform [31]. The specific objectives were:

(1) To construct a comprehensive 3D FEM model enabling the modeling of soil liquefaction and the seismic performance of the inclined pile groups with different configurations.
(2) To conduct parametric analyzes to evaluate the effects of different factors on the performance of the soil–pile system, including the pile inclination, the ground slope, the soil profile, and the amplitude of the input motion.
(3) Summarize the practical applications of inclined piles against liquefaction-induced lateral spreading.

The novelty of this research is that this study fills the gap left by previous inadequate investigations of inclined piles against liquefaction-induced spreading in the literature and provides insights into the effectiveness of inclined pile group configurations with the presence of liquefaction-induced lateral spreading.

2. Numerical Analysis Description

2.1. Problem Definition

The problem under consideration is a 1 × 2 pile group embedded in the sloping ground susceptible to liquefaction, as illustrated in Figure 1. The investigated parameters and their ranges are presented in Table 1. To explore the effects of inclinations of the left and right piles, three pile group configurations were analyzed with α_L and α_R ranging from 0° to 25°. These configurations include "IV" (an inclined left pile and a vertical right pile), "VI" (a vertical left pile and an inclined right pile), and "II" (two symmetrically inclined piles). Figure 1 depicts an example of configuration VI with $\alpha_L = 0°$ and $\alpha_R = 25°$. Additionally, the configuration with two vertical piles ($\alpha_L = \alpha_R = 0°$) was also analyzed for comparison purposes.

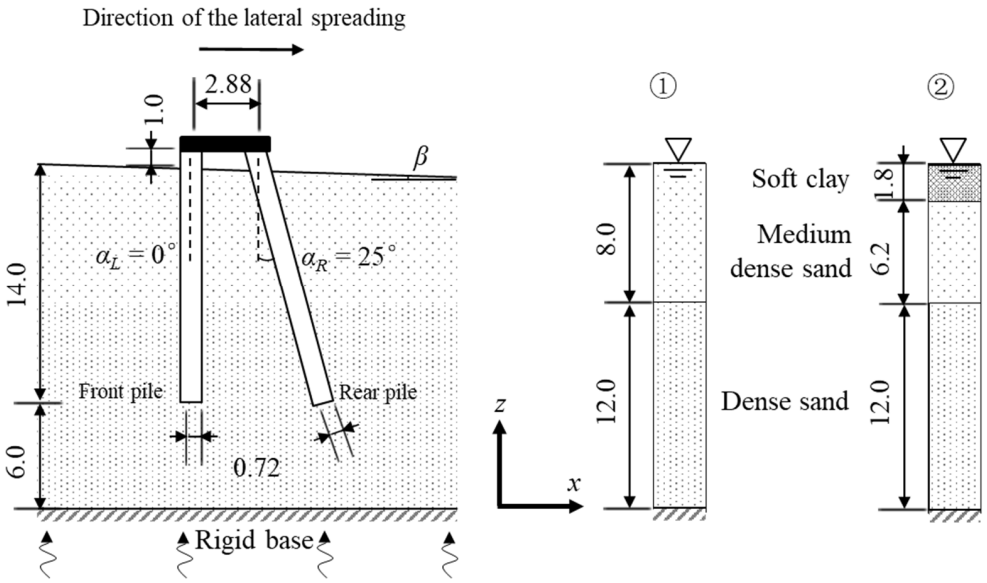

Figure 1. Schematic of model piles for configuration VI, with $\alpha_L = 0°$ and $\alpha_R = 25°$ and soil profiles (in meters).

Table 1. Ranges of the investigated factors in the parametric analysis.

Factor	Range
Peak base acceleration, $a_{max,base}$	0.1 g and 0.3 g
Inclination of left/front pile, α_L	0°, 5°, 10°, 15°, 20°, and 25°
Inclination of right/rear pile, α_R	0°, 5°, 10°, 15°, 20°, and 25°
Ground slope, β	0°, 2°, and 4°
Soil profile	① and ②

The piles were modeled to be elastic and have a diameter of D = 0.72 m, with a section stiffness of EI = 505 MN·m^2 (where E is the Young's modulus, and I is the moment of inertia). The pile spacing, i.e., the center-to-center distance between the two piles at the soil surface, is independent of the pile inclination and is fixed at four times the pile diameter, i.e., 4D = 2.88 m. The pile heads were connected by a rigid link with a lumped mass in the middle to simulate the cap (m_{cap} = 100 tons), which is 1.0 m above the soil surface. The depth of embedment of the pile group is 14.0 m, and the pile tips extend 6.0 m above the model base.

Two-layered soil deposits (Figure 1) on top of the rigid base were considered: (a) Profile ①: a fully saturated sandy soil deposit with the water level at the ground surface; and (b) profile ②: a soil deposit with an impermeable clay crust near the ground surface. The soil profile ① is composed of two soil layers: a dense sand layer (relative density D_r = 80%) with 12.0 m thickness at the bottom, and a medium-dense sand layer (D_r = 55%) with 8.0 m thickness on the top. On the other hand, the soil profile ② replaces the 1.8 m (i.e., 2.5D) thick medium-dense sand at the top with impervious soft clay. In addition to the level ground case (i.e., ground slope $\beta = 0°$), inclined ground (i.e., $\beta = 2°$ and 4°) has also been considered to induce lateral spreading towards the positive x-axis. The sloping ground is also adopted in other simulations and experiments (e.g., [22,32,33]) as one of the common methods to consider the influence of lateral spreading load on pile foundations. In OpenSees, a sloping ground could be modeled by inclining the direction of the gravitational force on the soil profile. The structure and pile in the model were still subjected to vertical gravitational force. Depending on the ground slope, the left and right piles can be called the front (upslope) and rear (downslope) piles, respectively.

The 1995 Kobe earthquake motion was used as the base input excitation but scaled to different amplitudes ($a_{max,base}$ = 0.1 g or 0.3 g). The acceleration time history and response spectrum shown in Figure 2a,c were normalized by the peak acceleration.

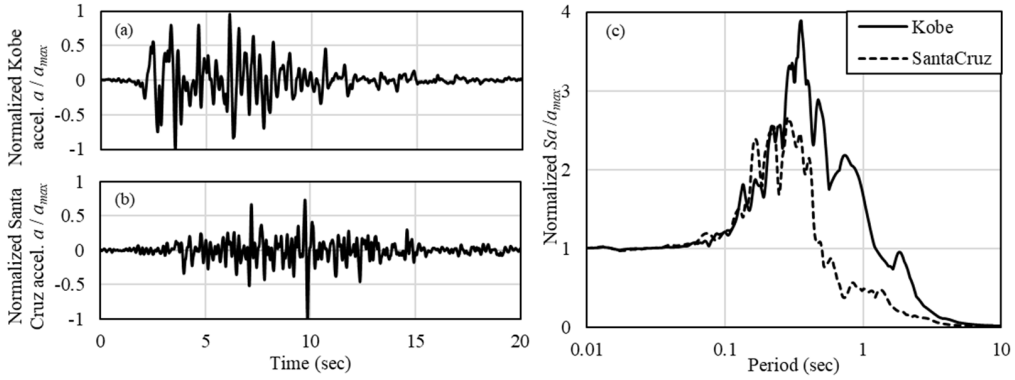

Figure 2. Input motions: (**a**) normalized Kobe acceleration time history; (**b**) normalized Santa Cruz acceleration time history; and (**c**) normalized response spectra.

2.2. Numerical Model Layout, Meshing, Boundary Conditions, and Analysis Settings

Due to symmetry, only half of the model was simulated, and the layout is shown in Figure 3, where a pile group with $\alpha_L = \alpha_R = 15°$ is displayed. The soil block is divided into a mesh consisting of 8 node SSPBrickUP elements and implemented with the *u-p* formulation [31]. The maximum allowable element height ($h_{\max}$) at each depth is determined from the shear wave velocity, V_s, via $h_{\max} = V_s/f_{\max}/4/4$, in which the maximum frequency content of the excitation $f_{\max}$ is conservatively set as 10 Hz, as suggested by Ramirez et al. [34]. According to Khosravifar et al. [15], V_s for sand is calculated through the relation $V_s = 85[(N_1)_{60} + 2.5]^{0.25}$, where the SPT $(N_1)_{60}$ value is estimated from the relation $(N_1)_{60} = 46D_r^2$. V_s for clay is calculated through the relation $V_s = 14.87c_u{}^{0.69}$, as suggested by L'Heureux and Long [35]. Additionally, soil elements are made finer in the vicinity of the piles. The distribution of the maximum allowable element height ($h_{\max,1}$ and $h_{\max,2}$ for sand and clay, respectively), and the actual element height (h) adopted in the analysis are also displayed in Figure 3. The adopted element size was deemed appropriate through a sensitivity analysis. The lateral extents of the soil in the x- and y-axes have been decided based on past modelling experiences with the 3D FEM analysis of piles that were subjected to lateral loads (e.g., [18,36]), and initial trial analyses were conducted to make sure the lateral extents were wide enough to eliminate the impact of the boundaries on the pile and the nearby soil. A total of 7866 soil elements and 9840 soil nodes were employed.

The model was fixed at the bottom against the three translational displacements (i.e., x, y, and z-axes). Nodes at the y = 0 and y = model width boundaries were fixed against the y-axis, while nodes with the same depths at the x = 0 and x = model length boundaries were constrained together and could move freely along the x-axis to simulate the laminar boundaries. Moreover, a free drainage boundary was considered at the ground surface.

In the dynamic simulations conducted in this study, viscous damping was applied through the Rayleigh formulation, where a damping ratio of 5% is considered. Moreover, a small amount of numerical damping was introduced to facilitate convergence through the integrator object in the OpenSees system. For this purpose, the Newmark integrator was employed, with a convergence parameter of 0.6 and a damping parameter of 0.3025. To expedite the convergence, the Krylov-Newton algorithm [31] was utilized. The norm displacement increment test [31] was utilized with a tolerance of 10^{-3} to verify the achievement of convergence. Finally, in the solution phase, SparseSYM [31] was used.

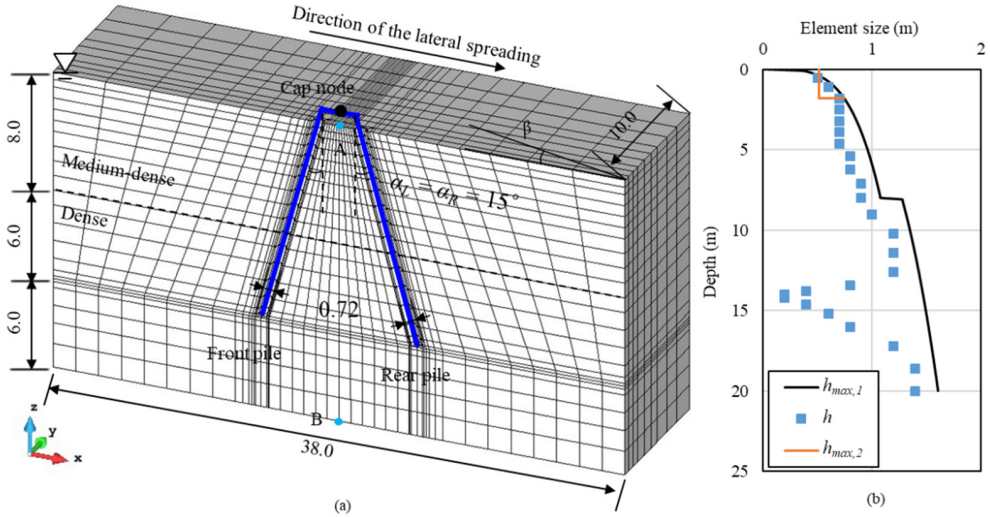

Figure 3. Typical representation for the parametric analysis: (**a**) model layout (in meters); and (**b**) element height profile.

2.3. Soil Constitutive Model

The Pressure-Dependent-Multi-Yield (PDMY02) material [31] was adopted to simulate the behavior of the sand. The PDMY02 material is suitable for simulating the undrained or partially drained cyclic response of liquefiable soils, and is frequently employed in the literature (e.g., [15,37,38]). The assumed PDMY02 parameters presented in Table 2 were derived from the method recommended by Khosravifar et al. [15] through linear interpolation of relative densities, as suggested by Kramer et al. [39]. Detailed definitions of this material can be found in the works by Yang et al. [37,38,40]. As according to Choobbasti and Zahmatkesh [41], constant permeability coefficients (k) of 3.70×10^{-5} m/s and 6.05×10^{-5} m/s were set for the dense and medium-dense sand layers, respectively.

An undrained cyclic triaxial test conducted by Arulmoli et al. [42] was simulated with the PDMY02 parameters for D_r = 57%, as recommended by Khosravifar et al. [15] (shown in Table 2). The test was conducted on Nevada sand with a relative density of about 60%, an effective confining pressure of 40 kPa, an offset deviatoric stress of 8.6 kPa, and a cyclic deviatoric stress of 26 kPa. Figure 4 presents the comparison between the numerical and experimental results. It can be seen that the negative axial strain, i.e., dilation, was significantly underestimated, and the variation of deviatoric stress at a high shear strain was not accurately simulated. This inaccuracy could result in the failure to simulate the momentary drops in excess pore pressure in centrifuge experiments. However, the developments of the excess pore water pressure (EPWP), and the positive axial strain (compression) were simulated properly by the PDMY02 material.

The pressure-independent multi-yield (PIMY) material [31] was adopted to simulate the characteristics of the clay. The material parameters were derived from Rahmani [43], in which layered clay was employed in simulating another centrifuge test of Wilson [44], and the pile responses were captured satisfactorily in the simulation. The clay layer was assumed to have low permeability, and $k = 1.0 \times 10^{-9}$ m/s was adopted in the numerical model.

Table 2. Material parameters for the PDMY02 and PIMY models.

Model Parameters	Sand (PDMY02)			Clay (PIMY)			
				0.0–1.5 m	1.5–3.0 m	3.0–4.5 m	4.5–6.1 m
D_r (%)	55	57	80	-	-	-	-
ρ (ton/m^3)	1.98	1.99	2.03	1.53	1.53	1.53	1.53
p_r (kPa)	100	100	100	100	100	100	100
G_r (MPa)	71.1	73.7	102.0	0.5	1.3	1.8	2.4
B_r (MPa)	189.5	196.8	272.1	2.33	6.1	8.4	11.2
c_u (kPa)	-	-	-	2.5	6.5	9.0	12.0
φ_f (°)	29.9	30.3	38.6	0.0	0.0	0.0	0.0
d	0.5	0.5	0.5	0.0	0.0	0.0	0.0
φ_{PT} (°)	24.9	25.3	31.8	-	-	-	-
c_1	0.022	0.019	0.003	-	-	-	-
c_2	3.2	3.2	1.0	-	-	-	-
c_3	0.2	0.2	0.2	-	-	-	-
d_1	0.15	0.15	0.27	-	-	-	-
d_2	3.0	3.0	3.0	-	-	-	-
d_3	0.0	0.0	0.0	-	-	-	-
liq_1	1.0	1.0	1.0	-	-	-	-
liq_2	0.0	0.0	0.0	-	-	-	-
γ_{max}	0.1	0.1	0.1	0.1	0.1	0.1	0.1
NYS	20	20	20	20	20	20	20
c	0.1	0.1	0.1	-	-	-	-
e	0.67	0.67	0.60	-	-	-	-

D_r: relative density; ρ: saturated density; p_r: reference pressure; G_r: reference shear modulus; B_r: reference bulk modulus; c_u: undrained shear strength, used as a numerical constant for sand; φ_f: friction angle at peak shear strength; d: pressure dependency coefficient; φ_{PT}: phase transformation angle; c_1, c_2, and c_3: contraction coefficients; d_1, d_2, and d_3: dilation coefficients; liq_1, and liq_2: liquefaction constants; γ_{max}: maximum shear strain; NYS: number of yield surface; c: numerical constant; and e: void ratio.

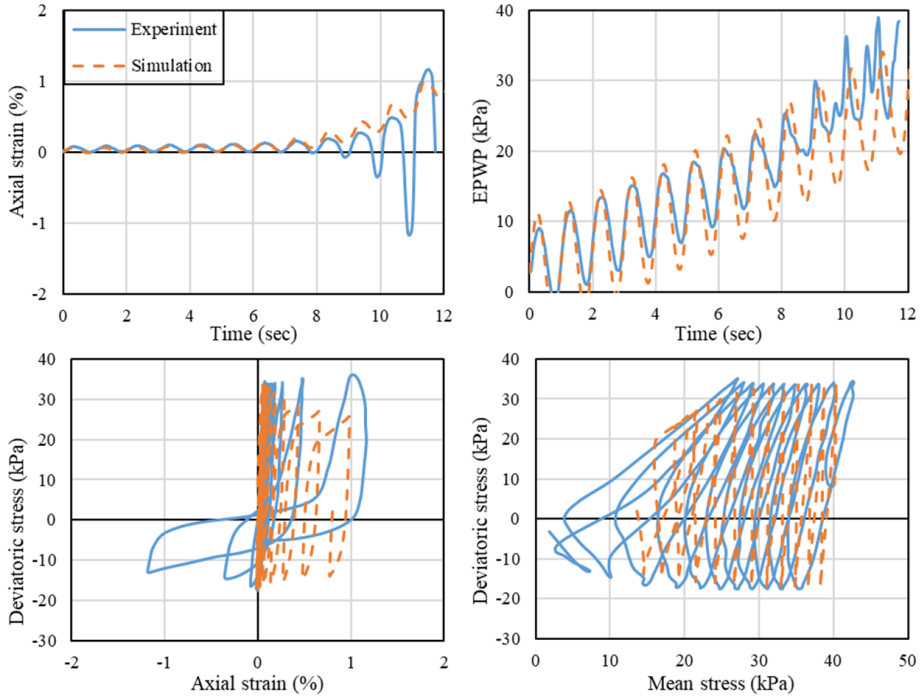

Figure 4. Comparison of undrained cyclic triaxial element responses between simulations in OpenSees and experiments by Arulmoli et al. [42].

2.4. Soil–Pile Interface Modeling

The piles were modeled as elastic beam-column elements. Based on the work by Cheng and Jeremić [22], a series of rigid links were bonded around the piles to shape the pile geometry. Interface elements were inserted between the rigid links and the surrounding soil nodes to enable the mobilization of the friction and separation mechanisms. The interface was characterized by zero cohesive strength, Coulomb friction with a friction coefficient of $\tan(2\varphi_f/3)$, in which φ_f is the friction angle of the sand, and with normal and tangential stiffnesses of $K_N = K_T = 1.0 \times 10^7$ kPa/m.

2.5. Model Validation

Prior to performing the numerical analysis, the model adopted needs to be validated. In the case of pile response in the soil profile ①, Wang and Orense [30,45] discussed the validation of the model, which indicated a satisfactory agreement between the pile response in saturated sand in the numerical analysis and the experimental data. As for soil profile ② with a soft clay crest layer, a centrifuge test (Csp5-C) performed by Wilson [43] was selected for the simulation. At the prototype scale, the soft clay layer on top has a thickness of 6.1 m, and the underlying sand layer with D_r = 80% has a thickness of 11.4 m. The Santa Cruz earthquake record from the 1989 Loma Prieta earthquake was scaled to 0.3 g accordingly and used as the base excitation. The normalized acceleration time history and spectrum were shown in Figure 2b,c, respectively. The sand and clay layers were simulated by the PDMY02 and PIMY materials, respectively, with the parameters shown in Table 2. According to Rahmani [43], different parameter values should be adopted for the clay layer at different depths.

Figure 5 compares the results of the simulation with the experiment, including the superstructure (SS) response, excess pore water pressure (EPWP) in the free field, and the bending moment of the pile at specific depths. The SS response is a measure of the structural behavior of the pile under seismic loading, and it is important for understanding the overall performance of the foundation system. EPWP is an indicator of soil liquefaction, and was examined at the depths of 0.7 m and 9.1 m below the ground surface. The bending moments, which represent the forces acting on the pile, were from the depths of 0.76 m and 1.52 m, respectively. In general, the numerical results and experimental data matched reasonably well, with the exception of the numerical model not satisfactorily capturing the fluctuations of the EPWP, especially in clay. The failure to adequately capture the transient drops in EPWP could be attributed to several reasons. Firstly, the PDMY02 material may have underestimated the dilatancy behavior of sand, as evidenced by previous studies [21,34]. Secondly, the PIMY material also lacks dilatancy formulations. These result in the insignificant expansion of soil under shear loading. Additionally, it has been noted by Wilson [44], that the records of the pore pressure in clay during the seismic loading of the experiment may not be reliable due to the response time and arching effects around the transducers [46]. Furthermore, the low and constant permeability of clay adopted in the numerical model may also be inconsistent with the situation in the experiments. Nevertheless, the fluctuations of EPWP in both clay and sand are relatively small, and they do not significantly affect the overall trend of the increase in EPWP. It is important to note that the current numerical study focuses on the responses of the sand and the pile, which the model has properly captured. Therefore, the current modeling method is deemed to be of acceptable accuracy, especially considering that the results of the 3D FEM analyzes in this study were mainly expressed as ratios of the maximum responses.

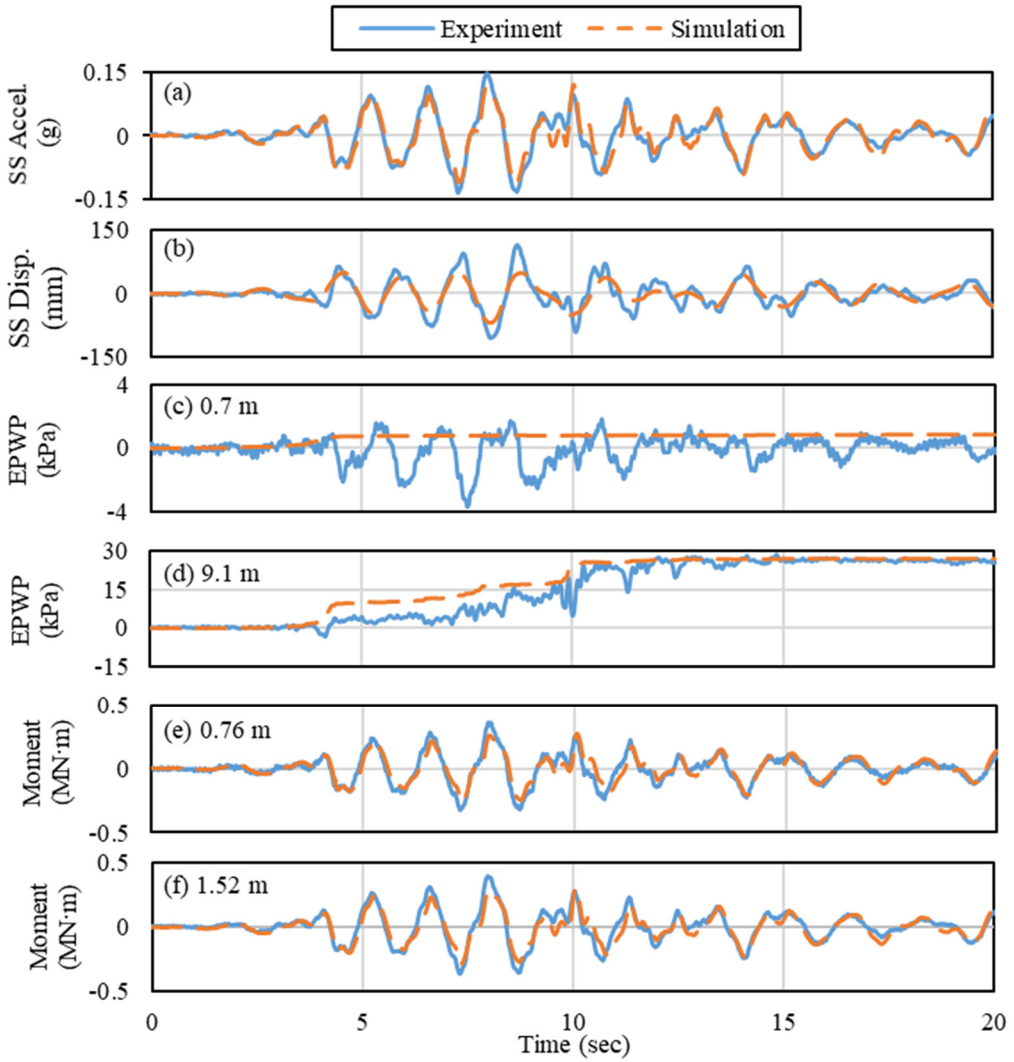

Figure 5. Comparison between the simulations in OpenSees and experiments conducted by Wilson [43]: (**a**) SS acceleration time history; (**b**) SS displacement time history; (**c**) EPWP at 0.7 m depth; (**d**) EPWP at 9.1 m depth; (**e**) bending moment at 0.76 m depth; and (**f**) bending moment at 1.52 m depth.

3. Analysis of the Results

Parametric analysis was performed to examine the seismic behavior of the 1 × 2 pile groups in the level and inclined soil profiles (Figure 1). In the analysis, the surface clay layer was modeled using the parameters for clay at depth 4.5 to 6.1 m (see Table 2) to simulate a much stiffer crust relative to that observed in the experiment. These things considered, seismic analyzes of the level and inclined ground without piles have also been conducted for comparison.

Based on the study reported by Li et al. [10,11], a performance index P (in percentage) was adopted to quantitatively evaluate the influence of a certain parameter:

$$P = \frac{Q_I - Q_V}{Q_V} \times 100\% \quad (1)$$

where Q_I and Q_V are the calculated values of the parameter for the inclined and vertical pile configurations, respectively. Hence, the performance of the inclined piles was able to be examined through the performance indices of the maximum system responses. For example, the performance index for the cap rotation can be calculated from the equation $P_\theta = (\theta_I - \theta_V)/\theta_V$, in which θ_I and θ_V are the maximum rotation of the cap when supported

by the inclined and vertical piles, respectively. Cap rotation refers to the angle between the horizontal axis and the connection line of the pile heads. A positive or negative value of P_θ can reflect the increase or decrease in the maximum cap rotation due to pile inclination, respectively. Hence, the performance index is an indicator of how each examined parameter was impacted by the inclination of the pile.

It is worth mentioning that other important factors, such as the diameter and nonlinearity of the pile, the pile spacing, the properties of the superstructure, the pile-to-cap connection, and the characteristics of the input motion, may also have considerable influences. However, such a comprehensive parametric study is beyond the scope of the current investigation.

3.1. Soil Response

In this study, the soil responses considered in our interpretation include the excess pore water pressure ratio (r_u, which is the ratio of excess pore water pressure and initial effective confining pressure), and the horizontal displacement (U_{soil}) at different depths. The vertical distributions of the maximum r_u in the free field (model boundaries are displayed in Figure 3) and at the soil center under the cap node (i.e., along the line AB in Figure 3) in the soil–pile interaction cases with vertical piles (i.e., $\alpha_L = \alpha_R = 0°$), are presented in Figure 6. In addition, the maximum lateral displacements of the corresponding model cases are shown in Figure 7. In both figures, the ground slope, the soil profile, and the amplitude of the base motion are shown in the legends. For instance, the case of "4S-②-0.3 g" indicates an inclined soil profile ② with a slope of 4° under excitation of $a_{max,base}$ = 0.3 g. Note that the depth indicated in the figure was measured from the ground surface. Moreover, the results for the non-liquefied soil profile ② are not shown, as they are similar to those observed in the non-liquefied soil profile ①.

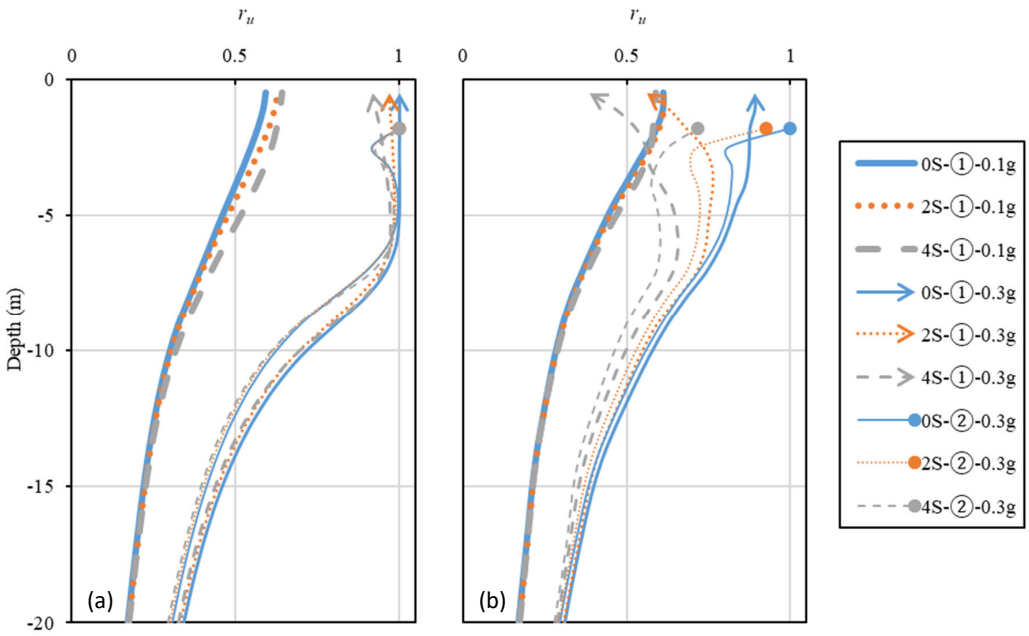

Figure 6. Distributions of the maximum r_u in (**a**) the free field; and (**b**) the soil center in models with vertical piles.

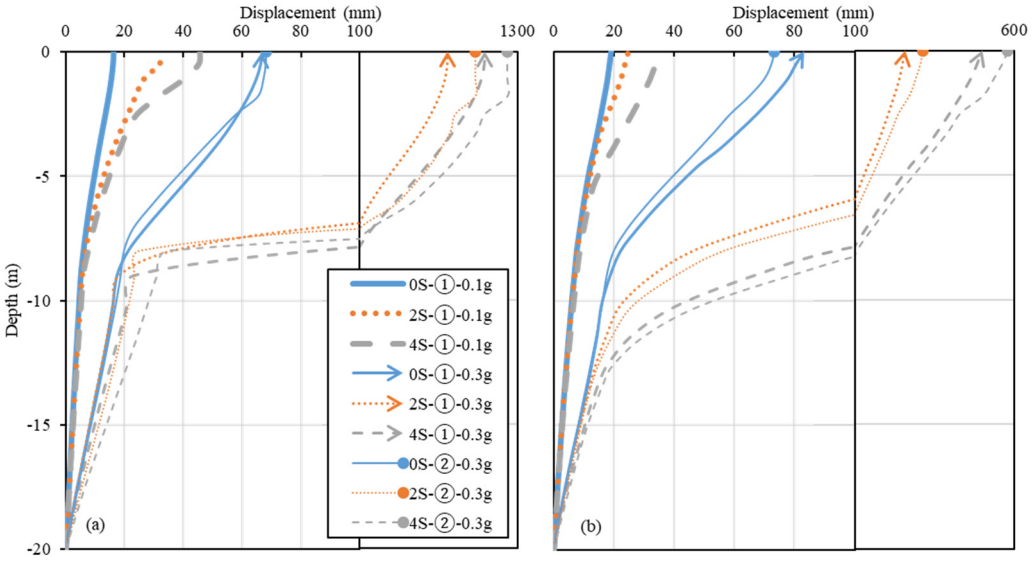

Figure 7. Horizontal displacement of soil (**a**) in free field; and (**b**) at the center of models with vertical piles.

It can be seen from Figure 6a that sandy soils at a shallower depth (up to 6 m) tend to liquefy (r_u = 1.0) for the two soil deposits under $a_{max,base}$ = 0.3 g (i.e., ①-0.3 g and ②-0.3 g cases). Under steeper slopes, the maximum r_u at the shallower depth is reduced slightly. The soil profile ① under a smaller amplitude (i.e., ①-0.1 g), however, does not liquefy, and the inclination of the ground resulted in a slight increase in r_u. Therefore, ①-0.1 g cases were considered as "non-liquefied" cases, while the rest were deemed as "liquefied" cases. As illustrated in Figure 6b, the maximum r_u in ①-0.1 g cases barely changes with the use of vertical piles. For cases under a larger amplitude, vertical piles reduce the maximum r_u all throughout the depth, which can be due to the strengthening effects of the pile groups on the soil. Therefore, the utilization of pile foundations can mitigate the occurrence of liquefaction. In addition,, abrupt increases in maximum r_u were observed on top of the medium-dense sand layer in the soil profile ②, which may be due to the resistance of the clay crust to drainage.

As shown in Figure 7, the maximum soil displacements in cases with a level ground or a smaller excitation amplitude were markedly smaller than those observed in other cases. In Figure 7a, a sharp increase in displacements was observed at 8 m depth, which was the interface of the two sand layers. These abrupt changes were mitigated partly by the presence of the vertical piles, as the displacements near the interface shown in Figure 7b changed moderately with the depth. The soil displacements at the clay-sand interface in the ②-0.3 g cases also demonstrated a slippage which may be attributed to the sharp increase in r_u shown in Figure 6. The presence of the pile group was found to increase the soil displacement in the level ground case, but also reduce that in the sloping ground case. The kinematic and inertial interactions of the soil–pile system can explain this phenomenon. In the level ground case, the inertial force generated by the cap during the dynamic loading dominates the soil displacement, resulting in increased soil displacements. In the sloping ground case, however, the kinematic effect becomes dominant, and the strengthening effects of the pile groups on the saturated ground decrease the soil displacements.

The distributions of the maximum r_u along line A-B in the level ground scenario are demonstrated in Figure 8. Only the results from configuration II were shown, as similar trends were observed in the other configurations. The increase in pile inclination reduces the maximum r_u in the upper zone of the medium-dense soil layer in Figure 8a,b, which may be caused by the reduced soil displacement displayed in Figure 9. It is worth mentioning that the reinforcement effects of the inclined piles on liquefiable soil deposits were also viewed in the shaking table tests performed by McManus et al. [13]. However,

the pile inclination enhances the development of maximum r_u at deeper depths, with the maximum r_u closer to 1.0 (Figure 8b,c). Similar to the observations seen in the flat ground case, the inclined piles were further away from the observation points, and thus the stiffening effect of the piles was weakened. Figure 9 shows the time histories of r_u and the horizontal displacement U_{soil} of the ground at different depths for the cases with soil profile ①, $a_{max,base}$ = 0.3 g, $\beta = 4°$, and $\alpha_L = \alpha_R = 0°$ and 25°. Although the rates of development of r_u at deeper depths were increased due to the presence of inclined piles, those of the U_{soil} at the corresponding depths were found to have significantly decreased. Therefore, the lateral stiffness of the whole soil–pile interaction system increased on the whole due to the utilization of the inclined piles. The increase in pile inclination may thereby only decrease the soil confinement in the middle part of the model.

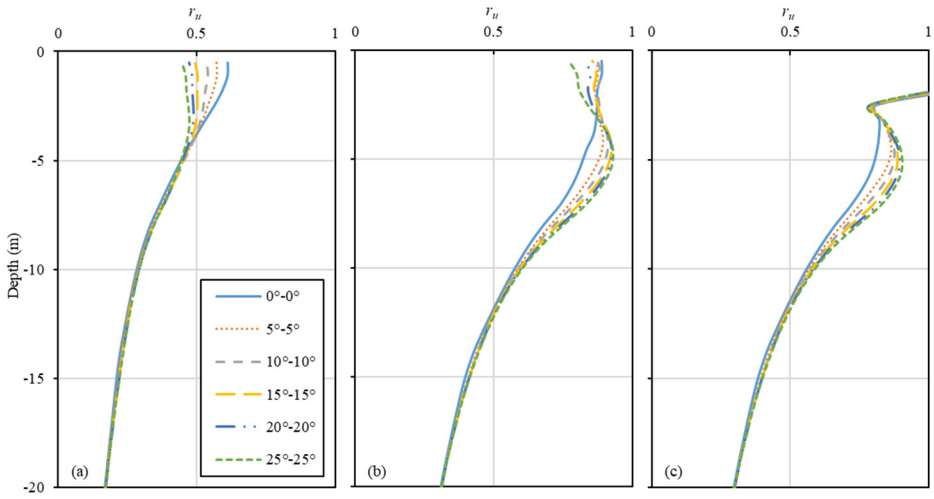

Figure 8. Distribution of the maximum r_u in level ground: (**a**) ①-0.1 g; (**b**) ①-0.3 g; and (**c**) ②-0.3 g.

Based on Equation (1), the performance indices for soil displacement, P_{Usoil}, were evaluated and subsequently illustrated in Figure 10. Note that the soil displacement in the analysis refers to the maximum displacement at Node A in Figure 3, which is at the ground surface and right below the cap node. The pile inclination α represents α_L, α_R, and $\alpha_L = \alpha_R$ for pile configurations IV, VI, and II, respectively. Most indices were negative, and showed decreasing tendencies with the pile inclination, which means that the use of inclined piles reduces the soil displacement, with larger pile inclinations boosting such positive effects. Indices for the sloping ground cases (Figure 10b,c) were even lower than those seen in the level ground cases (Figure 10a), indicating that inclined piles in the sloping ground have more noticeable positive effects than in the level ground. The positive effects of configuration VI (with P_{Usoil} being down to -50%) are more noticeable than those of configuration IV (with P_{Usoil} being down to −37%), but less noticeable than those of configuration II (with P_{Usoil} being down to −60%). The soil displacement seems to be reduced by the inclined piles, as the lateral stiffness of inclined pile groups was larger than that of the vertical pile groups. Moreover, the indices from the liquefied cases were generally smaller than those seen in the non-liquefied cases, demonstrating that inclined piles exhibit more noticeable beneficial effects when the soil liquefies. Therefore, pile groups with an inclined rear pile are more advantageous to the ground when considering the soil response.

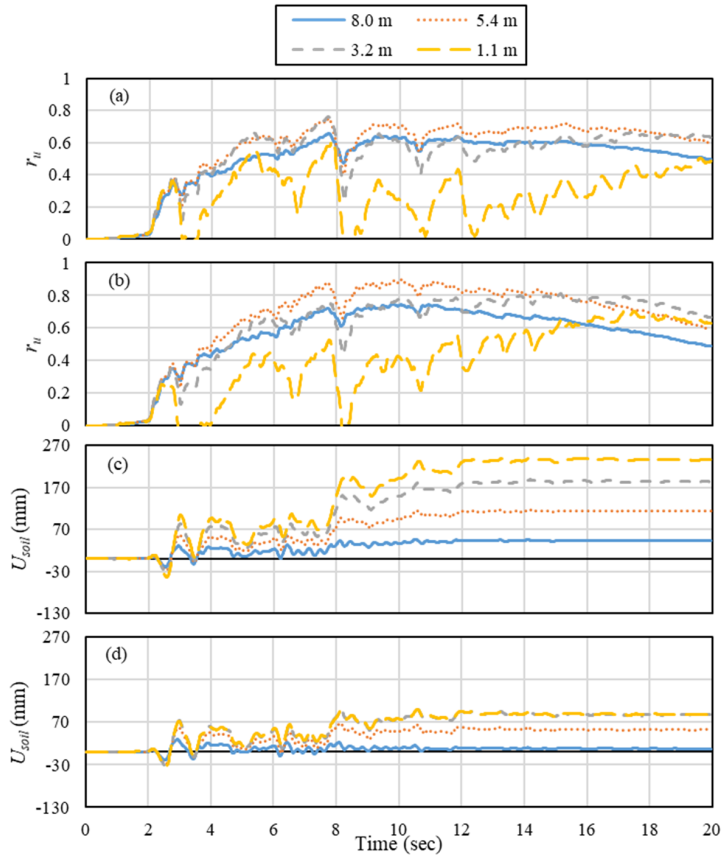

Figure 9. Soil response at different depths: (**a**) r_u for $\alpha = 0°$; (**b**) r_u for $\alpha = 25°$; (**c**) U_{soil} for $\alpha = 0°$; and (**d**) U_{soil} for $\alpha = 25°$.

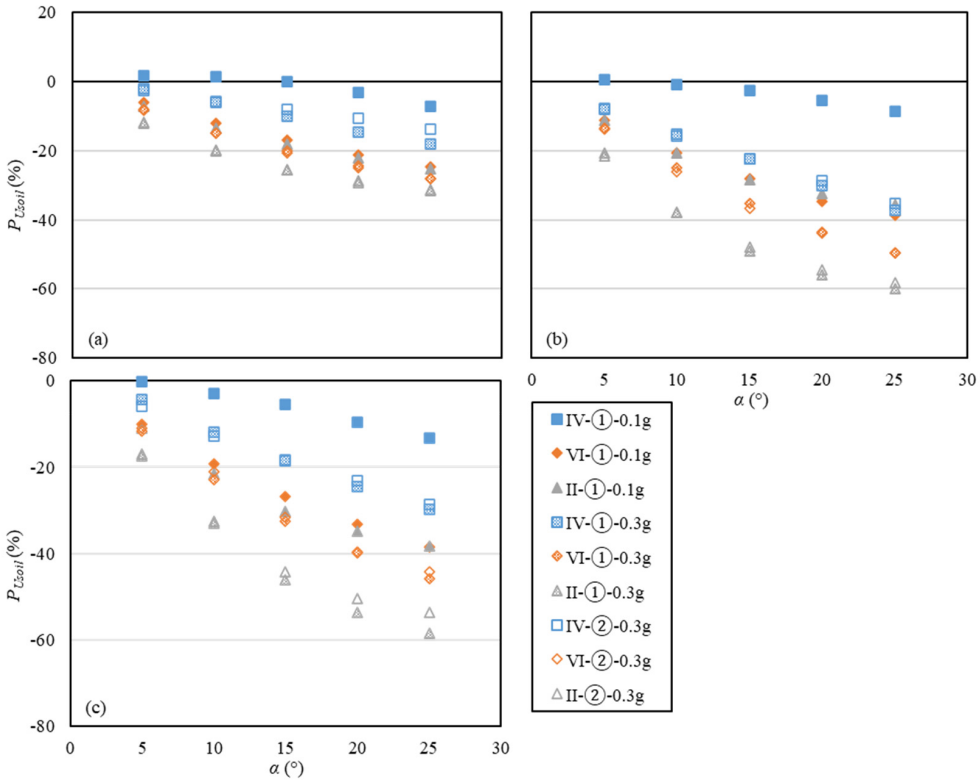

Figure 10. Performance index for the maximum soil displacement: (**a**) $\beta = 0°$; (**b**) $\beta = 2°$; and (**c**) $\beta = 4°$.

3.2. Cap Response

For the cap response, attention has been paid to the maximum inertial force ($F_I = m_{cap}a_{cap}$, in which a_{cap} is the horizontal acceleration of the cap), lateral displacement (U_{cap}), and rotation (θ, the rotation of the cap node is along the y-axis). The corresponding performance indices (i.e., P_{FI}, P_{Ucap}, and P_θ) are presented in Figures 11–13.

The values of P_{FI} for the level and sloping ground cases are shown in Figure 11. The utilization of pile configuration IV in the soil profile ② showed a detrimental effect in terms of the inertial force. Although configuration II in the soil profile ② shows a beneficial effect in level ground, this effect becomes detrimental in the sloping ground. Therefore, configuration VI displays more beneficial effects on soil profile ②. The negative indices from cases with the soil profile ① demonstrate that the maximum inertial force can be reduced due to the presence of inclined piles. Experiments by Li et al. [10,11] also illustrated similar beneficial effects. Moreover, this beneficial effect becomes less pronounced as the soil liquefies. Compared with the pile groups containing only one vertical pile, pile configuration II produces lower P_{FI}, representing more pronounced beneficial effects generally. For most situations, P_{FI} decreases with the pile rake angle. However, indices for configurations II and VI under a large amplitude of motion were either insensitive to or even decreased with pile inclinations that were larger than 15°.

As shown in Figure 12, indices for the cap deflection P_{Ucap} were found to be negative. This beneficial effect on the cap deflection has also been reported in other similar studies (e.g., [10,11,26,27,45]. Moreover, P_{Ucap} decreases with the pile inclination and soil liquefaction occurrence. The inclined piles were less beneficial in the level ground than in the sloping ground, as the indices shown in Figure 12b,c were lower than those observed in Figure 12a. Additionally, pile configurations II and VI showed more clear positive effects compared to configuration IV.

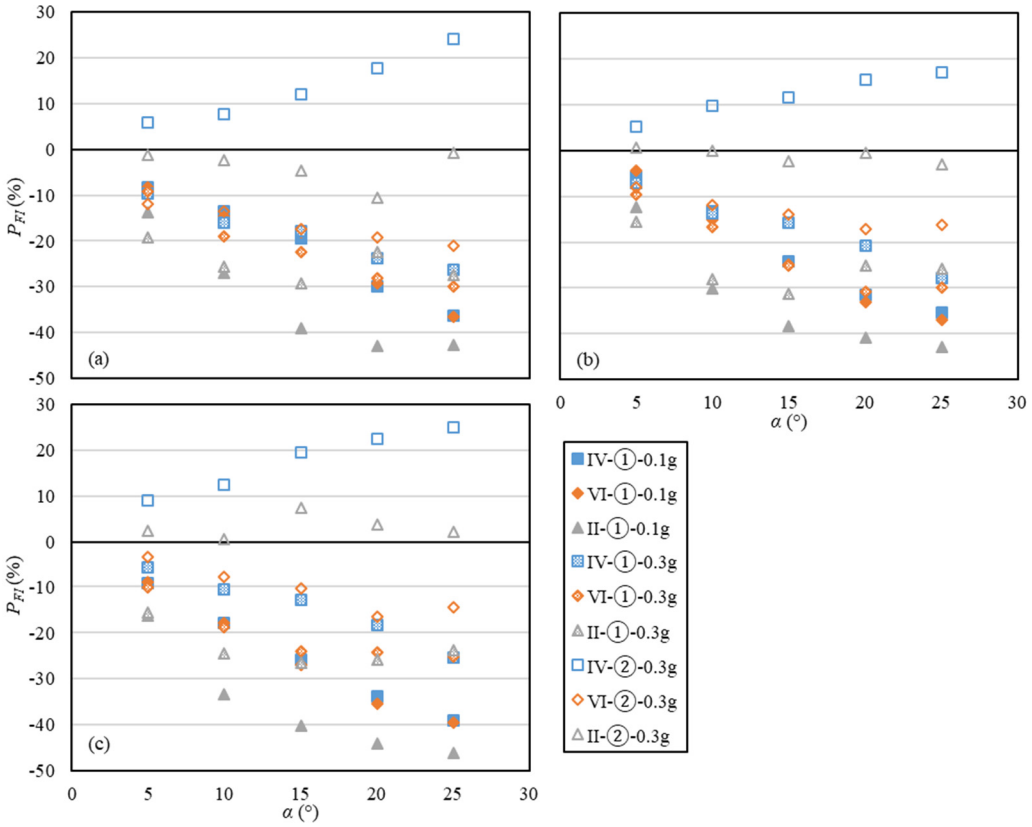

Figure 11. Performance index for the maximum inertial force: (**a**) $\beta = 0°$; (**b**) $\beta = 2°$; and (**c**) $\beta = 4°$.

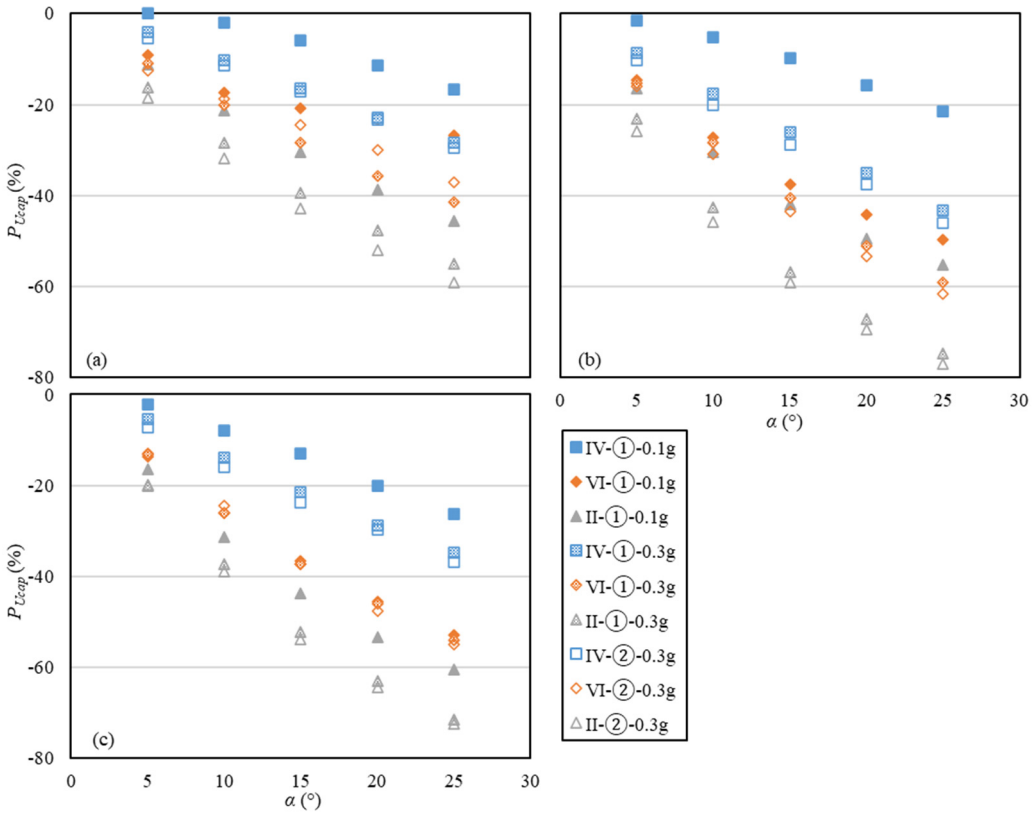

Figure 12. Performance index for the maximum cap deflection: (**a**) $\beta = 0°$; (**b**) $\beta = 2°$; and (**c**) $\beta = 4°$.

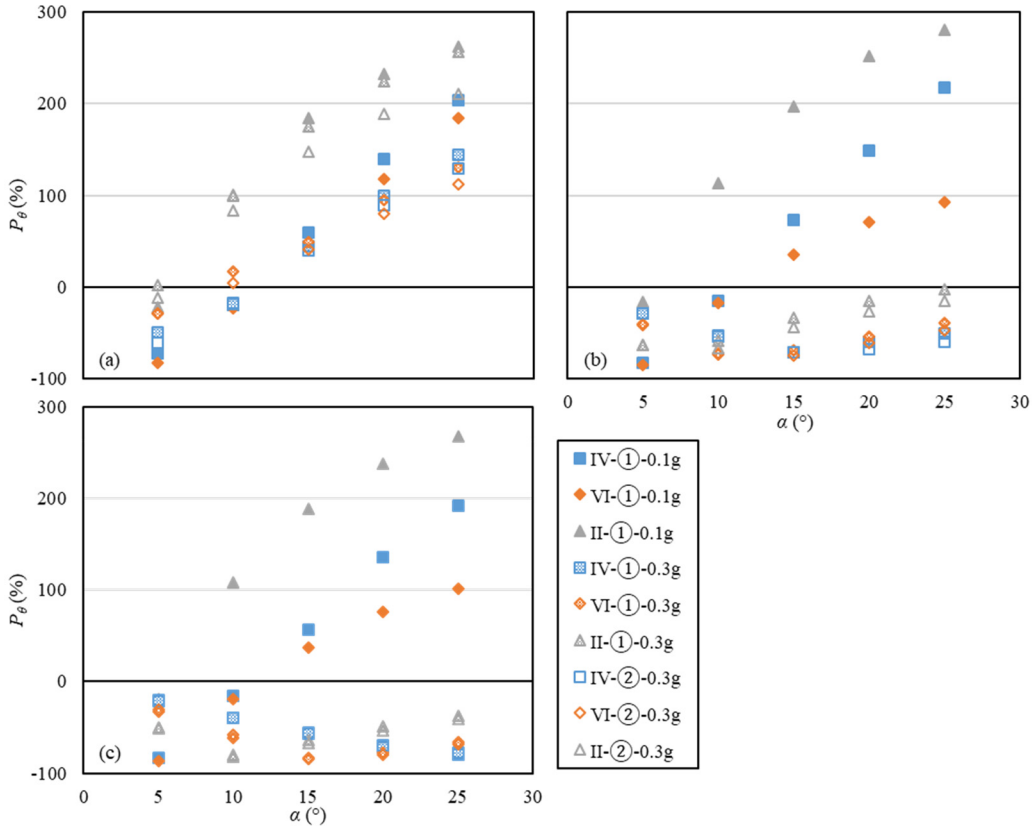

Figure 13. Performance index for the maximum cap rotation: (**a**) $\beta = 0°$; (**b**) $\beta = 2°$; and (**c**) $\beta = 4°$.

Figure 13 illustrates the P_θ for cases with different slopes. In level ground (Figure 13a), only the small pile inclinations ($\alpha < 10^\circ$) were able to reduce the cap rotation (e.g., P_θ for $\alpha = 5^\circ$ went down to −83%, while P_θ for $\alpha = 25^\circ$ went up to 256%). It has been noted that the utilization of inclined piles often produces significant cap rotation [10,26]. However, beneficial effects on cap rotation have been observed in the experiments of Li et al. [11], which may support the negative P_θ computed for cases with small pile inclinations. For the sloping ground cases, not only are the indices for the ①-0.3 g cases negative, but the positive indices for the other cases also decreased. Configurations IV and VI produce a lower P_θ than configuration II, except in the cases involving small pile inclinations ($\alpha < 10^\circ$) in liquefied sloping ground. These results show that, in terms of limiting the cap rotation, the combined use of the vertical and inclined piles is generally better than the symmetrically inclined pile groups.

In summary, pile inclination is beneficial in reducing the maximum inertial force and the lateral displacement of the cap in the level and sloping grounds (with P_{FI} being down to −46%, and P_{Ucap} down to −78%). Configuration II produced the lowest $P_{FI,}$ and an optimal pile inclination seems to exist at around 15°. Configurations VI and II were found to be more beneficial than configuration IV in reducing the cap deflection. With regard to the cap rotation, remarkable detrimental effects were observed, except for small pile inclinations ($\alpha \leq 10^\circ$) in the level ground and non-liquefied sloping ground cases. However, less detrimental effects were observed in the sloping ground case. Compared with configuration II, the combination of using the vertical and inclined piles together has more advantages in reducing the cap rotation.

3.3. Pile Response

The pile responses examined in this study include the maximum bending moment M, the shear force F_S, and the axial force F_A. Note that the negative axial forces (tension) may be generated during the seismic loading, which may damage concrete piles easily in a real-life scenario. Therefore, both the maximum and minimum axial forces were considered herein. The maximum pile deflection was not investigated here due to space limitation; however, it can be determined from either the bending moment distribution, or the shear stress distribution in the piles.

3.3.1. Maximum Bending Moment

Figure 14 illustrates the maximum bending moment profiles that developed in the inclined rear pile of configuration VI. The maximum bending moment generated on the piles increased considerably with the slope inclination. The maximum values generally occurred at the pile heads in the cases of the level ground (i.e., Figure 14a,d,g) and the non-liquefied sloping ground (i.e., Figure 14b,c). As displayed in the other figures, the peak bending moments in the piles with small inclinations occurred close to the bottom of the medium-dense soil layer. As the pile inclination increases, the bending moment at the pile heads and at the depths around the interface of soil layers generally decreases, especially in the liquefied cases. The decreased bending moment at the pile head has also been observed in the literature (e.g., [7,10,11,26]). According to Giannakou et al. [26], the prevalence of inertial loading results in smaller bending moments.

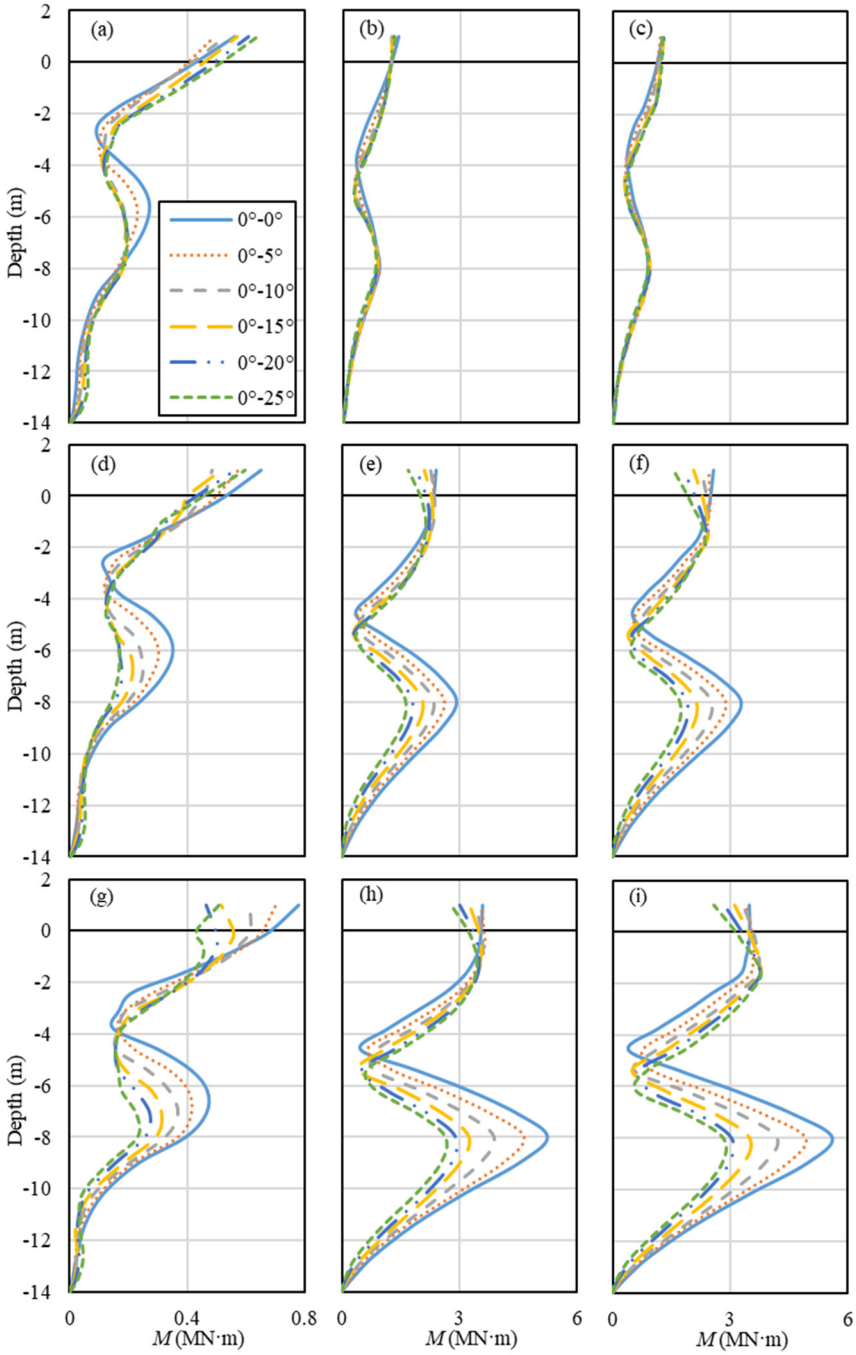

Figure 14. Distribution of the maximum bending moment in the rear pile for the pile configuration VI: (**a**) 0S-①-0.1 g; (**b**) 0S-①-0.3 g; (**c**) 0S-②-0.3 g; (**d**) 2S-①-0.1 g; (**e**) 2S-①-0.3 g; (**f**) 2S-②-0.3 g; (**g**) 4S-①-0.1 g; (**h**) 4S-①-0.3 g; and (**i**) 4S-②-0.3 g.

Figure 15 presents the performance index for the maximum bending moment P_M in both the front (Figure 15a–c) and rear piles (Figure 15d–f). In the non-liquefied level ground (0S-①-0.1 g), only configuration II results in a smaller maximum bending moment. In the sloping ground and liquefied level ground, however, both configurations VI and II were determined to be beneficial (with P_M being down to −35%). As for the liquefied cases, the presence of an impermeable crust exhibited minor effects on the bending moment. The beneficial effects of configurations VI and II became less pronounced (with P_M being down to −20%). As the pile inclination increases, generally more pronounced effects in the non-liquefied cases were induced, but this only had a minor impact in the liquefied cases.

As explained by Giannakou et al. [26], due to the significant stiffness ratio of piles to the liquefied soil, the additional stiffness provided by the pile inclination can only exhibit a minor influence on the system response.

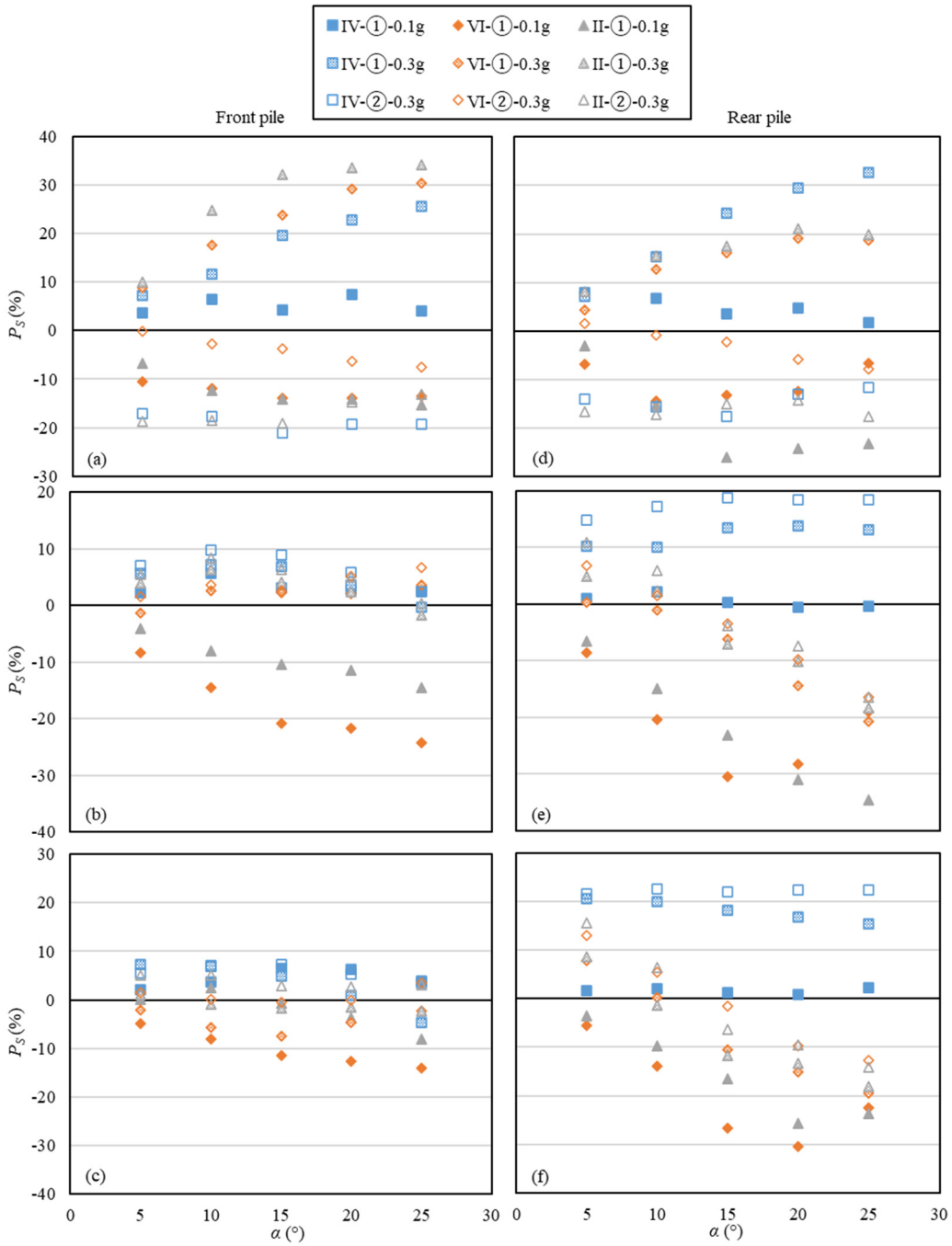

Figure 15. Performance index for the maximum bending moment: (**a**) front pile-0S; (**b**) front pile-2S; (**c**) front pile-4S; (**d**) rear pile-0S; (**e**) rear pile-2S; and (**f**) rear pile-4S.

Therefore, when considering the maximum bending moment, the utilization of asymmetric pile groups would be detrimental in non-liquefied level ground. In the presence of lateral spreading induced by liquefaction, pile group configurations VI and II are effective in decreasing the maximum bending moment in the piles.

3.3.2. Maximum Shear Force

Figure 16 illustrates the profiles of maximum shear force in the front pile of configuration II. It can be observed that the shear force profiles increase considerably with the increase in slope inclination. The locations of the peak maximum shear force along the piles were within the medium-dense soil layer. Abrupt changes in the distributions were observed at the interfaces of the soil layers, which were around 8 m and 1.8 m in the soil profile ②. These findings also correspond to the locations where noticeable changes in soil displacement profiles appear in Figure 7. As for the maximum shear force profiles, the pile inclination tends to amplify the maximum shear force at the pile head and the peak value at a lower location in the liquefied cases (i.e., Figure 16a,d,g), but tends to decrease those in the non-liquefied cases.

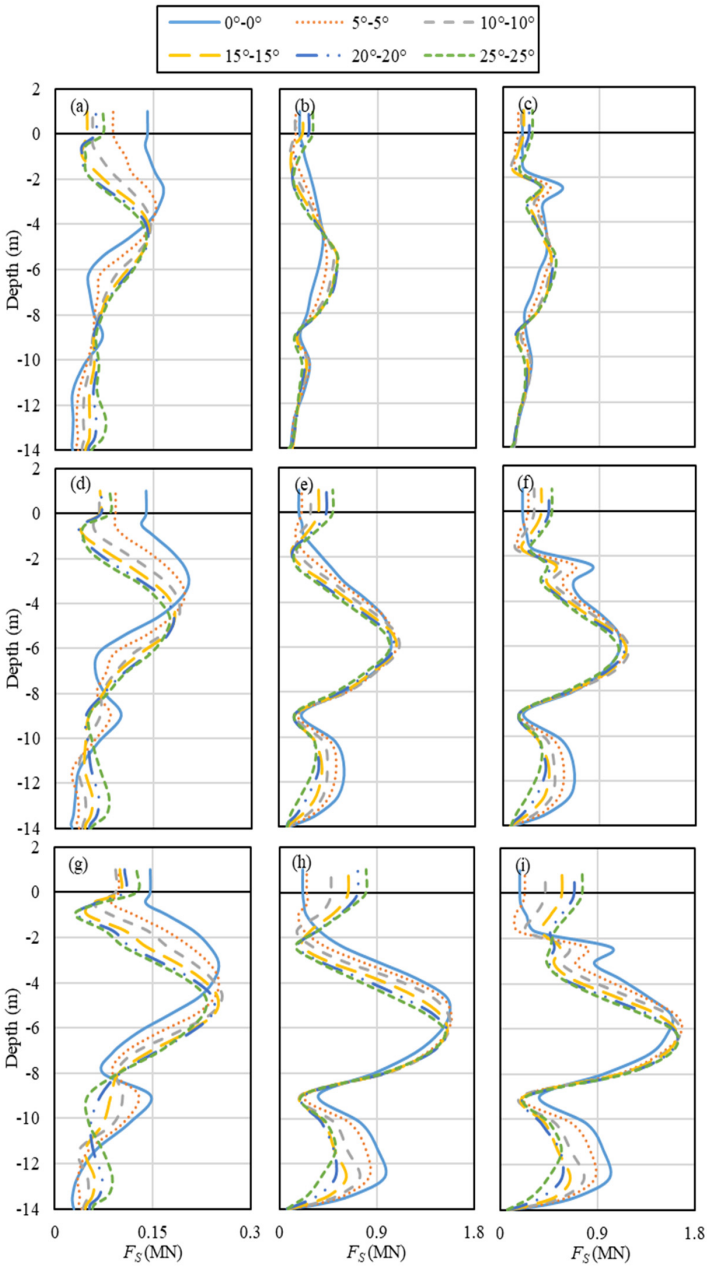

Figure 16. Distribution of the maximum shear force experienced by the front pile for the pile configuration II: (**a**) 0S-①-0.1 g; (**b**) 0S-①-0.3 g; (**c**) 0S-②-0.3 g; (**d**) 2S-①-0.1 g; (**e**) 2S-①-0.3 g; (**f**) 2S-②-0.3 g; (**g**) 4S-①-0.1 g; (**h**) 4S-①-0.3 g; and (**i**) 4S-②-0.3 g.

The performance indices corresponding to the maximum shear force P_S are demonstrated in Figure 17. In non-liquefied cases (i.e., ①-0.1 g), utilizing pile configurations VI and II is beneficial in decreasing the maximum shear force (with P_S being down to −34%). With a crust on the ground surface, the pile inclination generally plays a beneficial role, except for the front pile in the sloping ground. In the liquefied level ground without a crust, the use of the inclined piles amplifies the maximum shear force by around 34% at most. However, with the increase in the slope inclination, this negative effect becomes less noticeable, and even turns out to be positive, except for configuration IV. Compared with pile configuration IV, the other two configurations (i.e., VI and II) mainly exhibited beneficial effects, with the exception of the ①-0.3 g cases.

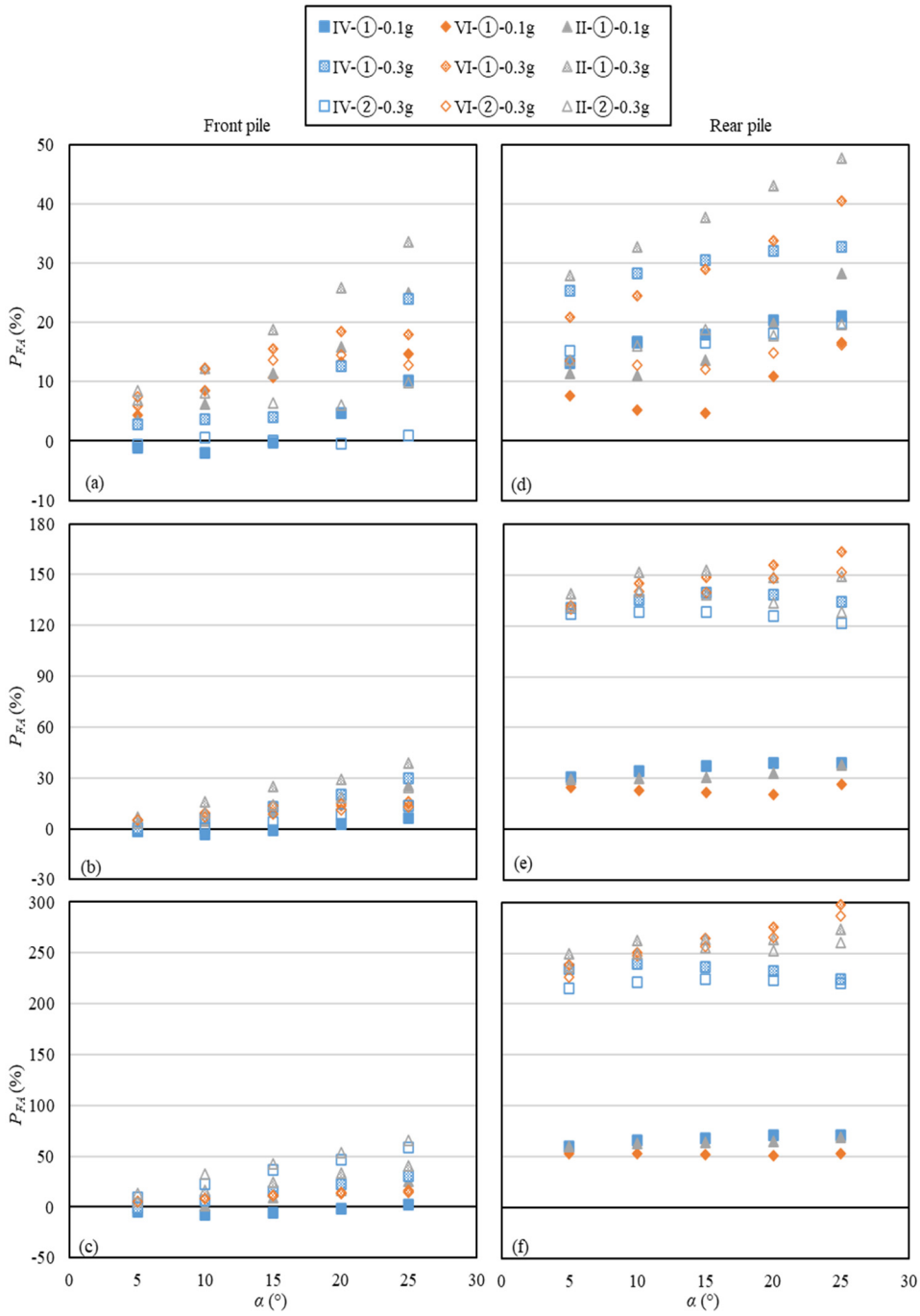

Figure 17. Performance index for the maximum shear force: (**a**) front pile-0S; (**b**) front pile-2S; (**c**) front pile-4S; (**d**) rear pile-0S; (**e**) rear pile-2S; and (**f**) rear pile-4S.

In summary, when considering the maximum shear force, the pile inclination in configurations VI and II has a positive effect in the sloping ground and non-liquefied level ground cases. With an impermeable crust on top, the utilization of inclined piles exhibits more beneficial effects with respect to the shear force.

3.3.3. Maximum Axial Force

Figure 18 illustrates the maximum axial force profiles for configuration VI in the sloping ground (β = 4°). For the vertical front piles, the peak compression force occurs at the pile heads. For the inclined rear pile, however, the peak values are in the vicinity of the bottom of the medium-dense soil layer. The pile inclination tends to increase the maximum axial force along the vertical piles. For the inclined piles, the pile inclination also amplifies the maximum axial force at depth but decreases that at the pile head. Giannakou et al. [26] observed even more significant reductions in the axial force at the pile head. The numerical simulations of Gerolymos et al. [7] and Sadek and Isam [47], also confirmed the amplification effect experienced by the piles in the deeper layer and put the blame on the lateral displacement of the soil. The sharp changes in the soil displacement profiles as shown in Figure 7 tend to support this explanation.

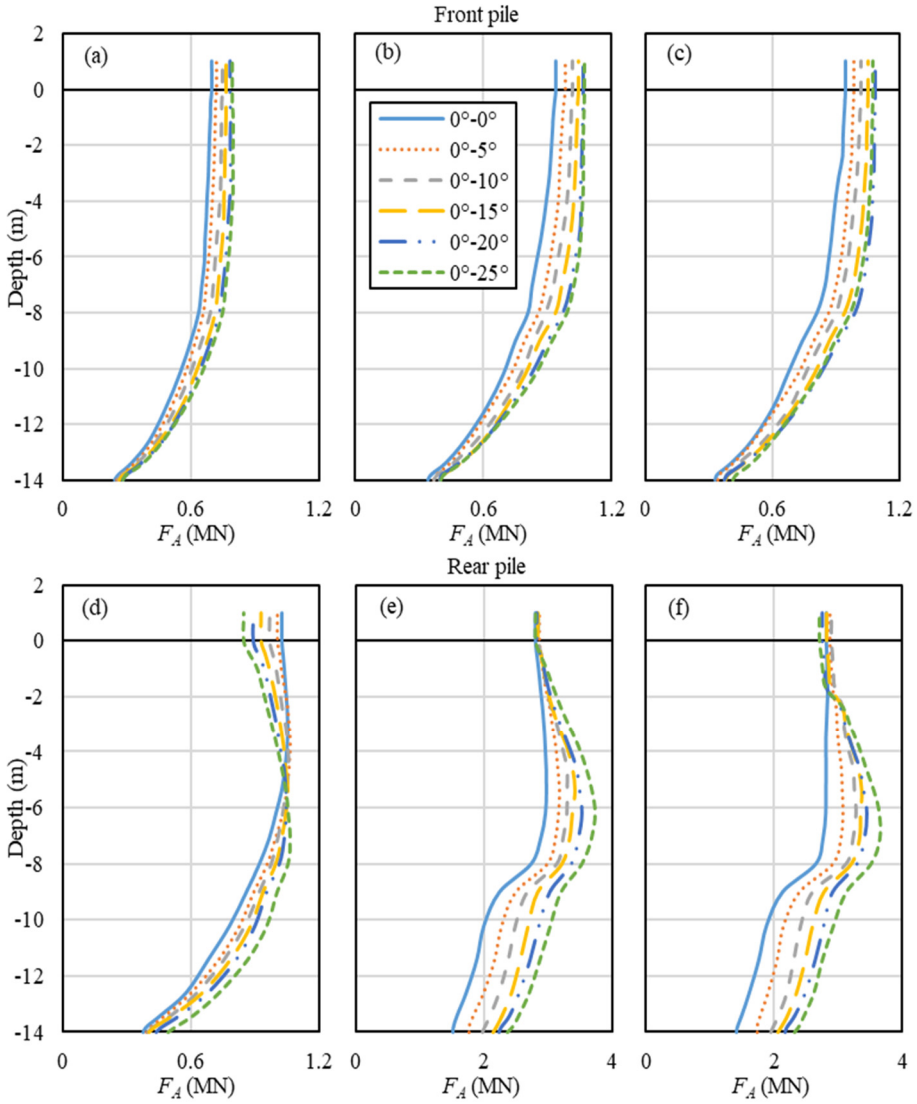

Figure 18. Distribution of the maximum axial force from the pile configuration VI in the sloping ground with β = 4°: (**a**) front pile-①-0.1 g; (**b**) front pile-①-0.3 g; (**c**) front pile-②-0.3 g; (**d**) rear pile-①-0.1 g; (**e**) rear pile-①-0.3 g; and (**f**) rear pile-②-0.3 g.

Figure 19 presents the performance index for the maximum axial force P_{FA}. Almost all indices were determined to be positive, except for the front pile for configuration IV in the ①-0.1 g cases. Inclined piles in the non-liquefied cases exhibited the lowest P_{FA}. With the presence of soil liquefaction and slope inclination, the detrimental effect of pile inclination becomes much more significant. Compared with the front pile (with P_{FA} being up to 82%), indices for the rear pile were much higher (with P_{FA} being up to 298%), especially for sloping ground cases. Additionally, configuration II commonly attracted larger axial forces compared to the other pile groups containing only one inclined pile.

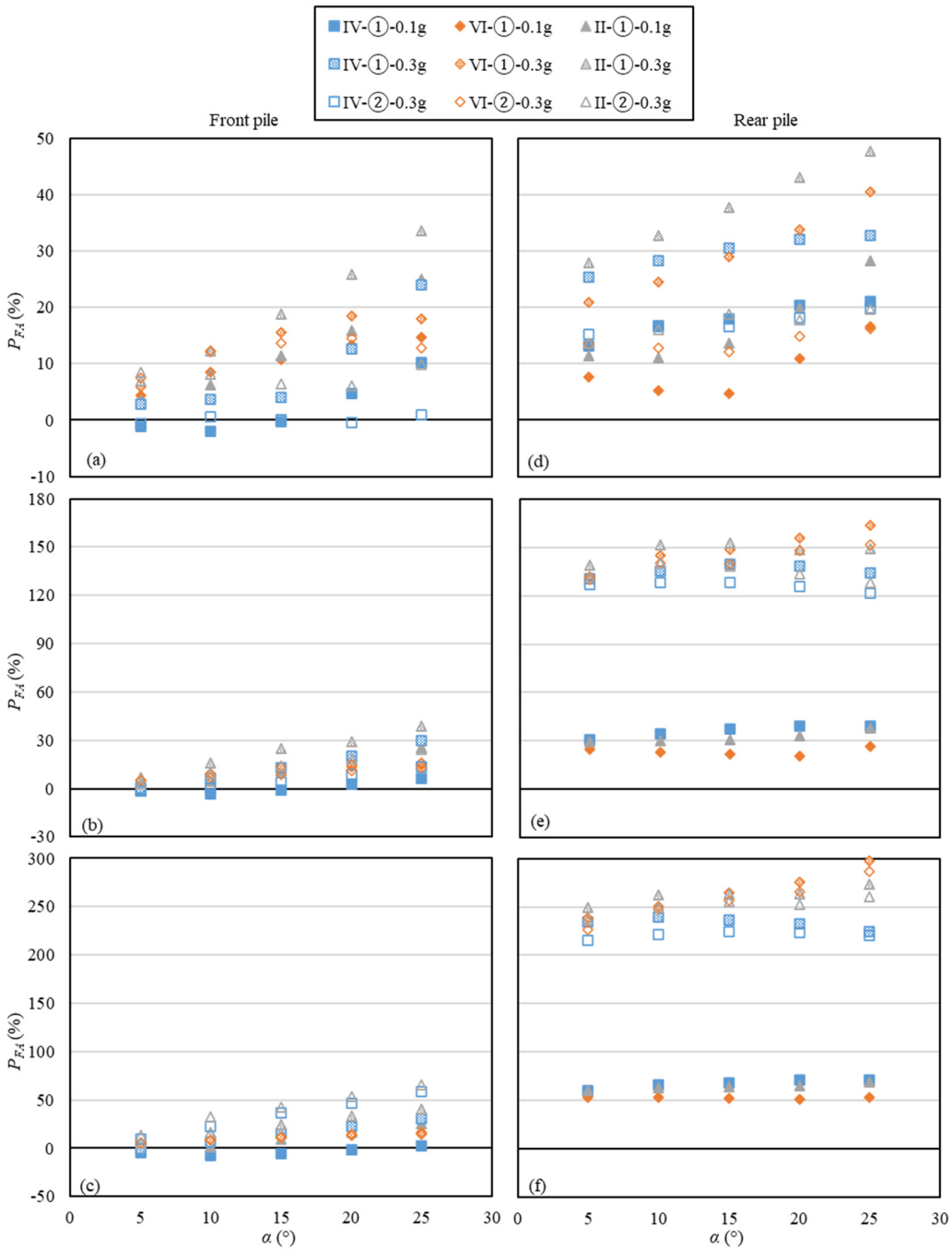

Figure 19. Performance index for the maximum axial force: (**a**) front pile-0S; (**b**) front pile-2S; (**c**) front pile-4S; (**d**) rear pile-0S; (**e**) rear pile-2S; and (**f**) rear pile-4S.

3.3.4. Minimum Axial Force

Figure 20 demonstrates the minimum axial force profiles experienced by the front pile of configurations VI and II in the sloping ground with $\beta = 4°$. It can be observed that extensive negative axial forces or tensile forces have been generated due to the occurrence of soil liquefaction. Compared with the front pile, the rear pile has not experienced significant tensile forces, and was thus not presented in Figure 20. The presence of the impermeable crust had negligible effects on the minimum axial force. Although the negative F_A on the vertical pile can be eliminated as the pile inclines, the negative axial forces on the inclined piles were amplified in most cases. Therefore, inclined piles are not appropriate to be used when considering the tensile axial force. As the minimum F_A in the vertical piles may be close to zero, the computed performance indices will be predicted to be exceptionally high. Hence, the performance indices were not used in analyzing the minimum F_A.

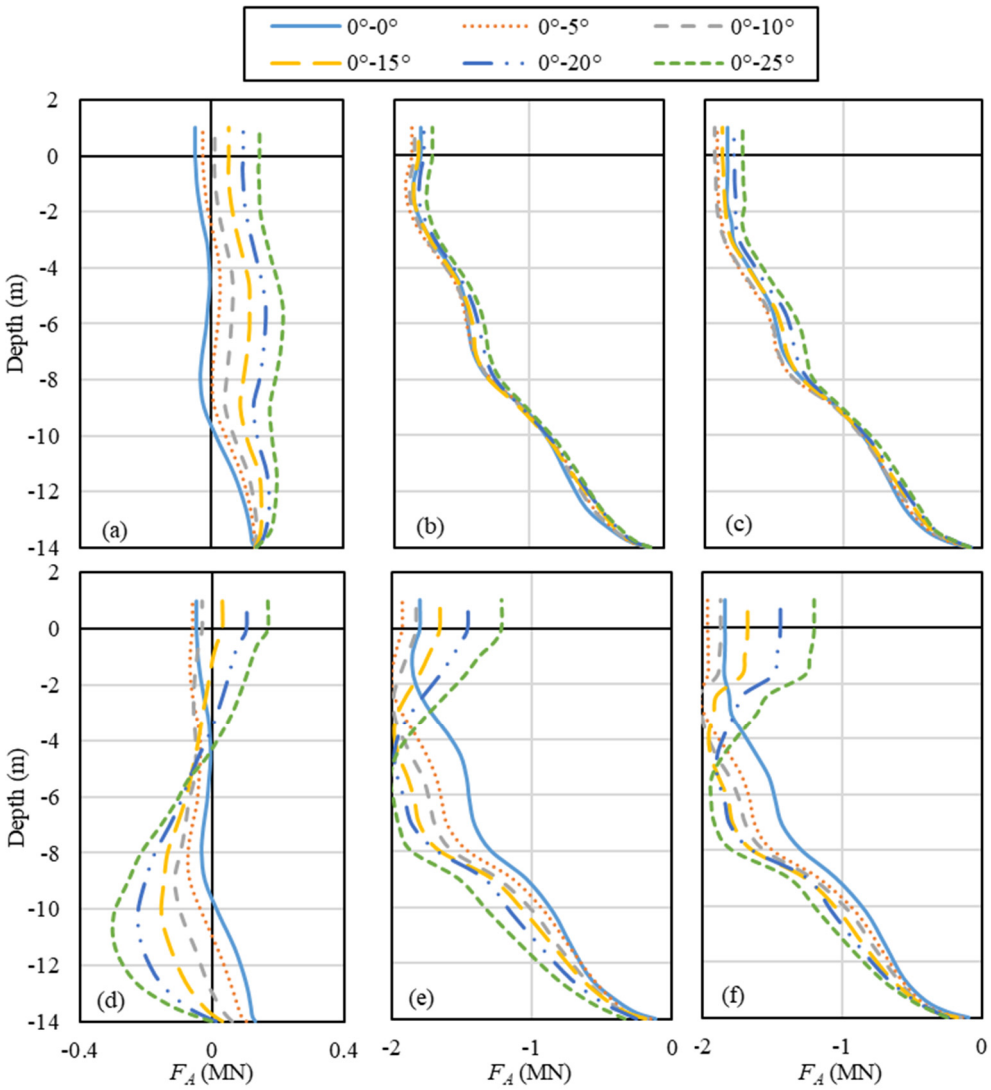

Figure 20. Distribution of the minimum axial force experienced by the front pile in the sloping ground with $\beta = 4°$: (**a**) VI-①-0.1 g; (**b**) VI-①-0.3 g; (**c**) VI-②-0.3 g; (**d**) II-①-0.1 g; (**e**) II-①-0.3 g; and (**f**) II-②-0.3 g.

Thus, the pile inclination normally increases the peak maximum axial force, and more considerable increases can be detected as the soil liquefies, or when lateral spreading is induced. Compared with the front pile, which is close to the top of the slope, the detrimental effects of the inclinations of the rear pile are more pronounced. As for the minimum axial

force along the pile, the use of inclined piles generally results in the development of larger tensile forces.

4. Discussion

In the parametric analysis, several factors, including pile inclination, ground slope, and soil liquefaction occurrence, were investigated for a specified model configuration and input motion. Based on the results, the systematic performance of the inclined piles against lateral spreading can be examined. The results demonstrated that inclined piles could outperform vertical piles in reducing soil deformation and the cap response, including inertial force, lateral displacement, and rotation. This beneficial effect is consistent with the experiments conducted by Li et al. [10,11]. The presence of an impermeable crust on top of the liquefiable soil layer magnifies the soil–pile responses, but only exhibits non-significant impacts on the effects of the inclined piles on the system, except for the total base shear force. Regarding the pile responses, such as the bending moment, the shear force, and the axial force, the performance of the inclined piles depends on the pile group configuration. Inclined piles were found to decrease the bending moment at the pile head, which is consistent with previous literature (e.g., [7,10,11,26]). This study also confirms the reduction in the axial force at the pile head, as previously reported by Giannakou et al. [26].

Pile inclinations ranging from 0° to 25° were investigated within the scope of the current paper. Generally, the beneficial or detrimental effects of inclined piles vary with the increase in pile rake angle. However, there are still some situations in which there is an optimal inclination, which is between 0° and 15°, considering the balance between the beneficial or detrimental effects. Hence, in real projects, an appropriate pile inclination should be adopted to magnify the beneficial effects and minimize or even remove the detrimental effects of inclined piles.

There are three pile group configurations investigated herein. Based on the indices of the system responses, configuration IV, which comprises a vertical rear pile and an inclined front pile, was found to be unsuitable for use in the sloping ground. Under the influence of soil liquefaction, and slope and pile inclinations, either configurations II or VI perform better in terms of the different system responses. Therefore, using inclined pile groups with an inclined rear pile could maximize the efficiency of the inclined pile groups. However, it should be noted that the axial compressional force experienced by this inclined pile could be notably enlarged. Therefore, additional mitigations can be adopted with respect to the compression properties of the pile, whilst still benefiting from the advantageous effects of the inclined piles.

5. Conclusions and Recommendations

To justify the beneficial or detrimental effects of using inclined piles in sloping ground, this paper examined the seismic behavior of the inclined piles against lateral spreading induced by liquefaction using a parametric 3D FEM analysis. The main conclusions can be drawn below:

- In the sloping ground case, better performance can be obtained with the use of two pile group configurations, “II” (two symmetrically inclined piles), and “VI” (the combination of a vertical front pile and an inclined rear pile).
- In the non-liquefied ground scenario, the utilization of inclined piles with appropriate configurations can be beneficial to most of the soil–pile system responses, except for the cap rotation and the axial force (either compression or tension) on the pile. Conversely, inclined piles with small inclinations can also be beneficial for cap rotation.
- In the liquefied level ground scenario, inclined piles were found to be detrimental to the maximum pore water pressure in the near-field soil, and in the cap rotation, shear force, and axial force (either compression or tension) on the pile.
- In the liquefied sloping ground scenario, in which a large lateral spreading has been induced, inclined piles become beneficial in reducing the rotation of the cap and the shear force on the pile. Moreover, pronounced beneficial effects were observed in

the displacement of the soil and cap, bending moment, and cap rotation. As for the compressive and tensile axial forces, however, the detrimental effects were amplified significantly for the large ground inclinations.

- Compared with the non-liquefied scenario, inclined piles in the liquefied ground case could have more pronounced beneficial effects on the lateral displacement of the soil and cap, and less pronounced detrimental effects on the cap rotation. However, there were also more pronounced detrimental effects on the axial compression or tension on the pile, and less pronounced beneficial effects on the inertial force under the cap, as well as the bending moment and shear force on the pile.

Within the scope and conditions examined in this study, the utilization of inclined piles with suitable configurations can generally result in better performance of the soil–pile–cap system. With the occurrence of liquefaction-induced lateral spreading, the performance of the inclined pile groups tends to be better than that in the level ground case, except for the fact that the additional compression demand on the pile should be met.

It is important to note that the results of this study are subject to certain limitations imposed by the constitutive models and numerical models used. Specifically, the soil constitutive model employed tends to underestimate the post-liquefaction settlement in sandy soils, and the pile group configurations investigated may not be fully representative of all practical applications. Additionally, while the parametric analysis did include several significant factors, other important variables that can affect the performance of inclined piles include the pile diameter, pile nonlinearity, stiffness of the pile cap, natural frequency of the superstructure, properties of the input motion, and permanent lateral loading or ground deformation. Therefore, a more developed constitutive model is recommended, more comprehensive investigations should be performed, and, when possible, physical model tests or case studies should be integrated to formulate design guidelines for future use in practice.

Author Contributions: Conceptualization: Y.W. and R.P.O.; methodology: Y.W. and R.P.O.; software: Y.W.; validation: Y.W. and R.P.O.; formal analysis and interpretation: Y.W. and R.P.O.; writing: Y.W. and R.P.O. All authors have read and agreed to the published version of the manuscript.

Funding: This research received no external funding.

Data Availability Statement: Some or all data supporting the findings of this study are available from the corresponding author upon reasonable request.

Acknowledgments: The authors would like to thank the China Scholarship Council (CSC), the University of Auckland Joint Doctoral Scholarship, and the contribution of NeSI high-performance computing facilities in this research. New Zealand's national facilities are provided by the NZ eScience Infrastructure and funded jointly by NeSI's collaborator institutions and through the Ministry of Business, Innovation & Employment's Research Infrastructure Program (https://www.nesi.org.nz).

Conflicts of Interest: The authors declare no conflict of interest.

Nomenclature

The following notations were used in this manuscript:

$(N_1)_{60}$	SPT value
a_{cap}	Horizontal acceleration of the cap
$a_{max,base}$	Peak base acceleration
B_r	Reference bulk modulus
c	Numerical constant
c_u	Undrained shear strength
c_1, c_2, c_3	Contraction coefficients
d	Pressure dependency coefficient
D	Pile diameter
d_1, d_2, d_3	Dilation coefficients
D_r	Relative density

e	Void ratio
F_A	Maximum axial force in pile
F_I	Maximum inertial force on pile
f_{max}	Maximum frequency content of the excitation
FS	Maximum shear force in pile
G_r	Reference shear modulus
h_{max}	Element height
k	Permeability of soil
liq_1, liq_2	Liquefaction constants
M	Maximum bending moment in pile
m_{cap}	Mass of the cap
NYS	Number of yield surface
p_r	Reference pressure
P_{usoil}, P_θ, P_{FI}, P_{ucap}, P_M, P_{FA}	Performance indices for different quantities
r_u	Excess pore water pressure ratio
U_{soil}, U_{cap}	Horizontal displacements of soil and cap
V_s	Shear wave velocity
α_L	Inclination of left/front pile
α_R	Inclination of right/rear pile
β	Ground slope
γ_{max}	Maximum shear strain
θ	Maximum rotation of the cap
ρ	Saturated soil density
φ_f	Friction angle at peak shear strength
φ_{PT}	Phase transformation angle

References

1. Seed, R.B.; Dickenson, S.E.; Idriss, I.M. Principal geotechnical aspects of the 1989 Loma Prieta earthquake. *Soils Found.* **1991**, *31*, 1–26. [CrossRef]
2. Finn, W.D.L.; Fujita, N. Piles in liquefiable soils: Seismic analysis and design issues. *Soil Dyn. Earthq. Eng.* **2002**, *22*, 731–742. [CrossRef]
3. AFPS (Association Française de Génie Parasismique). *Association Francaise de Genie Parasismique Recommandations*; Presses del Ponts at Chausseés: Paris, France, 1990.
4. *EN 1998-5:2004*; Eurocode 8: Design of Structures for Earthquake Resistance Part 5: Foundations, Retaining Structures and Geotechnical Aspects. CEN (European Committee for Standardization): Brussels, Belgium, 2004.
5. Haskell, J.; Madabhushi, S.; Cubrinovski, M.; Winkley, A. Lateral spreading-induced abutment rotation in the 2011 Christchurch earthquake: Observations and analysis. *Géotechnique* **2013**, *63*, 1310–1327. [CrossRef]
6. Pender, M.J. Aseismic pile foundation design analysis. *Bull. New Zealand Soc. Earthq. Eng.* **1993**, *26*, 49–160. [CrossRef]
7. Gerolymos, N.; Giannakou, A.; Anastasopoulos, I.; Gazetas, G. Evidence of beneficial role of inclined piles: Observations and summary of numerical analyses. *Bull. Earthq. Eng.* **2008**, *6*, 705–722. [CrossRef]
8. Berrill, J.B.; Christensen, S.A.; Keenan, R.P.; Okada, W.; Pettinga, J.R. Case study of lateral spreading forces on a piled foundation. *Géotechnique* **2001**, *51*, 501–517. [CrossRef]
9. Escoffier, S.; Chazelas, J.-L.; Garnier, J. Centrifuge modelling of raked piles. *Bull. Earthq. Eng.* **2008**, *6*, 689–704. [CrossRef]
10. Li, Z.; Escoffier, S.; Kotronis, P. Centrifuge modeling of batter pile foundations under earthquake excitation. *Soil Dyn. Earthq. Eng.* **2016**, *88*, 176–190. [CrossRef]
11. Li, Z.; Escoffier, S.; Kotronis, P. Centrifuge modeling of batter pile foundations under sinusoidal dynamic excitation. *Bull. Earthq. Eng.* **2015**, *14*, 673–697. [CrossRef]
12. Tazoh, T.; Sato, M.; Jang, J.; Taji, Y.; Gazetas, G.; Anastasopoulos, I. Kinematic Response of Batter Pile foundation: Centrifuge tests. In *Soil-Foundation-Structure Interaction*; Orense, R., Chouw, N., Pender, M., Eds.; Taylor and Francis Group: London, UK, 2010; pp. 41–47. [CrossRef]
13. McManus, K.; Turner, J.; Charton, G. Inclined reinforcement to prevent soil liquefaction. In Proceedings of the Annual NZSEE Technical Conference, Wairakei, New Zealand, 11–13 March 2005.
14. Shahrour, I.; Juran, I. Seismic behaviour of micropile systems. *Proc. Inst. Civ. Eng. Ground Improv.* **2004**, *8*, 109–120. [CrossRef]
15. Khosravifar, A.; Boulanger, R.W.; Kunnath, S.K. Effects of liquefaction on inelastic demands on extended pile shafts. *Earthq. Spectra* **2014**, *30*, 1749–1773. [CrossRef]
16. Shafieezadeh, A.; Desroches, R.; Rix, G.J.; Werner, S.D. Seismic Performance of Pile-Supported Wharf Structures considering Soil-Structure Interaction in Liquefied Soil. *Earthq. Spectra* **2012**, *28*, 729–757. [CrossRef]

17. Wang, S.; Orense, R.P. Modelling of raked pile foundations in liquefiable ground. *Soil Dyn. Earthq. Eng.* **2014**, *64*, 11–23. [CrossRef]
18. McGann, C.R.; Arduino, P.; Mackenzie-Helnwein, P. Applicability of Conventional *p-y* Relations to the Analysis of Piles in Laterally Spreading Soil. *J. Geotech. Geoenvironmental Eng.* **2011**, *137*, 557–567. [CrossRef]
19. Cubrinovski, M.; Uzuoka, R.; Sugita, H.; Tokimatsu, K.; Sato, M.; Ishihara, K.; Tsukamoto, Y.; Kamata, T. Prediction of pile response to lateral spreading by 3-D soil–water coupled dynamic analysis: Shaking in the direction of ground flow. *Soil Dyn. Earthq. Eng.* **2008**, *28*, 421–435. [CrossRef]
20. Li, G.; Motamed, R. Finite element modeling of soil-pile response subjected to liquefaction-induced lateral spreading in a large-scale shake table experiment. *Soil Dyn. Earthq. Eng.* **2017**, *92*, 573–584. [CrossRef]
21. Chang, D.; Boulanger, R.; Brandenberg, S.; Kutter, B. FEM Analysis of Dynamic Soil-Pile-Structure Interaction in Liquefied and Laterally Spreading Ground. *Earthq. Spectra* **2013**, *29*, 733–755. [CrossRef]
22. Cheng, Z.; Jeremić, B. Numerical modeling and simulation of pile in liquefiable soil. *Soil Dyn. Earthq. Eng.* **2009**, *29*, 1405–1416. [CrossRef]
23. Abu-Farsakh, M.; Souri, A.; Voyiadjis, G.; Rosti, F. Comparison of static lateral behavior of three pile group configurations using three-dimensional finite element modeling. *Can. Geotech. J.* **2018**, *55*, 107–118. [CrossRef]
24. Hazzar, L.; Hussien, M.N.; Karray, M. Numerical investigation of the lateral response of battered pile foundations. *Int. J. Geotech. Eng.* **2017**, *11*, 376–392. [CrossRef]
25. Xie, Y.; Huo, Y.; Zhang, J. Development and validation of p-y modeling approach for seismic response predictions of highway bridges. *Earthq. Eng. Struct. Dyn.* **2017**, *46*, 585–604. [CrossRef]
26. Giannakou, A.; Gerolymos, N.; Gazetas, G.; Tazoh, T.; Anastasopoulos, I. Seismic Behavior of Batter Piles: Elastic Response. *J. Geotech. Geoenvironmental Eng.* **2010**, *136*, 1187–1199. [CrossRef]
27. Sadek, M.; Shahrour, I. Influence of the head and tip connection on the seismic performance of micropiles. *Soil Dyn. Earthq. Eng.* **2006**, *26*, 461–468. [CrossRef]
28. Sarkar, R.; Roy, N.; Serawat, A. A Three Dimensional Comparative Study of Seismic Behaviour of Vertical and Batter Pile Groups. *Geotech. Geol. Eng.* **2018**, *36*, 763–781. [CrossRef]
29. Rajeswari, J.S.; Sarkar, R. Seismic response of batter piles in liquefiable soils. In Proceedings of the 7th International Conference on Earthquake Geotechnical Engineering, Rome, Italy, 17–20 June 2019.
30. Wang, Y.; Orense, R.P. Numerical analysis of inclined pile group performance in liquefiable sands. In Proceedings of the 7th International Conference on Earthquake Geotechnical Engineering, Rome, Italy, 17–20 June 2019.
31. Mazzoni, S.; McKenna, F.; Scott, M.H.; Fenves, G.L.; OpenSees Command Language Manual. Pacific Earthquake Engineering Research (PEER) Center. 2007. Available online: http://opensees.berkeley.edu/OpenSees/manuals/usermanual/OpenSeesCommandLanguageManual.pdf (accessed on 16 April 2021).
32. Janalizadeh, A.; Zahmatkesh, A. Lateral response of pile foundations in liquefiable soils. *J. Rock Mech. Geotech. Eng.* **2015**, *7*, 532–539. [CrossRef]
33. Zhang, S.; Wei, Y.; Cheng, X.; Chen, T.; Zhang, X.; Li, Z. Centrifuge modeling of batter pile foundations in laterally spreading soil. *Soil Dyn. Earthq. Eng.* **2020**, *135*, 106166. [CrossRef]
34. Ramirez, J.; Barrero, A.R.; Chen, L.; Dashti, S.; Ghofrani, A.; Taiebat, M.; Arduino, P. Site Response in a Layered Liquefiable Deposit: Evaluation of Different Numerical Tools and Methodologies with Centrifuge Experimental Results. *J. Geotech. Geoenvironmental Eng.* **2018**, *144*, 04018073. [CrossRef]
35. L'Heureux, J.S.; Long, M. Correlations between shear wave velocity and geotechnical parameters in Norwegian clays. In Proceedings of the 17th Nordic Geotechnical Meeting, Reykjavik, Iceland, 25–28 May 2016.
36. Li, Z.; Kotronis, P.; Escoffier, S.; Tamagnini, C. A hypoplastic macroelement for single vertical piles in sand subject to three-dimensional loading conditions. *Acta Geotech.* **2016**, *11*, 373–390. [CrossRef]
37. Yang, Z.; Elgamal, A.; Parra, E. Computational Model for Cyclic Mobility and Associated Shear Deformation. *J. Geotech. Geoenvironmental Eng.* **2003**, *129*, 1119–1127. [CrossRef]
38. Yang, Z.; Lu, J.; Elgamal, A.; OpenSees Soil Models and Solid-Fluid Fully Coupled Elements: User's Manual. San Diego. 2008. Available online: https://citeseerx.ist.psu.edu/viewdoc/download?doi=10.1.1.520.3689&rep=rep1&type=pdf (accessed on 29 August 2021).
39. Kramer, S.L.; Arduino, P.; Shin, H. *Using OpenSees for Performance-based Evaluation of Bridges on Liquefiable Soils*; PEER Report 2008/07; Pacific Earthquake Engineering Research Center, University of California: Berkeley, CA, USA, 2008.
40. Yang, Z. Numerical Modelling of Earthquake Site Response Including Dilation and Liquefaction. Ph.D. Dissertation, Columbia University, New York, NY, USA, 2000.
41. Choobbasti, A.J.; Zahmatkesh, A. Computation of degradation factors of p-y curves in liquefiable soils for analysis of piles using three-dimensional finite-element model. *Soil Dyn. Earthq. Eng.* **2016**, *89*, 61–74. [CrossRef]
42. Arulmoli, K.; Muraleetharan, K.K.; Hossain, M.M.; Fruth, L.S. *VELACS (Verifications of Liquefaction Analyses by Centrifuge Studies) Laboratory Testing Program*; Soil Data Report; The Earth Technology Corporation: Virginia Beach, VA, USA, 1992. [CrossRef]
43. Rahmani, A. Three-dimensional Nonlinear Analysis of Dynamic Soil-Pile-Structure Interaction for Bridge Systems under Earthquake Shakings. Ph.D. Dissertation, The University of British Columbia, Victoria, BC, Canada, 2014.
44. Wilson, D.W. Soil-Pile-Superstructure Interaction in Liquefying Sand and Soft Clay. Ph.D. Dissertation, University of California, Davis, Oakland, CA, USA, 1998.

45. Wang, Y.; Orense, R.P. Numerical analysis of seismic performance of inclined piles in liquefiable sands. *Soil Dyn. Earthq. Eng.* **2020**, *139*, 106274. [CrossRef]
46. Knodel, P.; Kutter, B.; Sathialingam, N.; Herrmann, L. Effects of Arching on Response Time of Miniature Pore Pressure Transducer in Clay. *Geotech. Test. J.* **1990**, *13*, 164. [CrossRef]
47. Sadek, M.; Isam, S. Three-dimensional finite element analysis of the seismic behavior of inclined micropiles. *Soil Dyn. Earthq. Eng.* **2004**, *24*, 473–485. [CrossRef]